# MEMS and Additively Manufactured Micro-Mechanical Isolators

by

Arthur Gernt Bond III

A Thesis submitted to the Graduate Faculty of
Auburn University
in partial fulfillment of the
requirements for the Degree of
Master of Science

Auburn, Alabama
August 8, 2020

Keywords: isolators, transmissibility, natural frequency,
resonant frequency, accelerometer, attenuation

Approved by

Robert Dean, Chair, Professor of Electrical & Computer Engineering
Mark Adams, Associate Professor of Electrical & Computer Engineering
John Hung, Professor of Electrical & Computer Engineering
Thaddeus Roppel, Associate Professor of Electrical & Computer Engineering
Edmon Perkins, Assistant Professor of Mechanical Engineering

Abstract

The purpose of the research effort was the development and evaluation of mechanical isolators. Some MEMS sensors have a known vulnerability to high frequency vibrations in various environments. The nature of the vulnerability was characterized through literature. A theoretical solution to combat the vulnerability was developed and packaged into devices known as mechanical isolators. Two mechanical isolators were developed. Both isolators shared similar functionality but were greatly different in execution. The isolator concepts were evaluated through simulations and adjusted to exhibit desirable behavior. Each concept was fabricated by its respected means. The fabricated prototypes were evaluated in simulated conditions with the use of a mechanical shaker and a laser vibrometer. Secondary damping components were introduced and served to aid in isolator performance. Certain configurations of the isolators were found to provide the sensor with adequate isolation from high frequency vibration inducing environments.

Table of Contents

Abstract ........ 1

Table of Contents ........ 2

List of Figures ........ 3

Introduction ........ 4

Mission Objection ........ 5

Background and Problem ........ 5

Theoretical solution ........ 15

Parameters ........ 20

Design ........ 20

Simulation ........ 26

Fabrication ........ 33

Testing ........ 57

Results ........ 62

Conclusion ........ 70

Future Work ........ 71

References ........ 72

# List of Figures

Figure 1: Accelerometer ... 5
Figure 2: Accelerometer Integrated Circuit ... 6
Figure 3: Base Excitation Model ... 8
Figure 4: Gain vs Frequency Ratio Plot ... 14
Figure 5: Electrostatic Actuator ... 16
Figure 6: Responses ... 17
Figure 7: Isolator Sum Response ... 17
Figure 8: Mechanical Isolator ... 18
Figure 9: I3 Isolator ... 22
Figure 10: I9 Isolator ... 22
Figure 11: Printed Isolator ... 24
Figure 12: Isolator w/ Damping Element ... 25
Figure 13: I3 w/ Proof Mass ... 27
Figure 14: I9 w/ Proof Mass ... 27
Figure 15: Printed Isolator w/ Proof Mass ... 28
Figure 16: FEA Boundaries Setup ... 28
Figure 17: FEA Silicon Material Properties ... 29
Figure 18: FEA Resin Material Properties ... 30
Figure 19: FEA I3 Results ... 31
Figure 20: FEA I9 Results ... 31
Figure 21: FEA Printed Isolator Results ... 32
Figure 22: Fabrication Process Flow ... 34
Figure 23: Raw Silicon Wafer ... 36
Figure 24: SOI Wafer Material Profile ... 36
Figure 25: Oxidation Thickness vs Time ... 40
Figure 26: Wafer Oven ... 41
Figure 27: Wafer Spinner ... 43
Figure 28: Mask Aligner ... 44
Figure 29: Wafer Mask ... 44
Figure 30: Wafer w/ Photoresist ... 46
Figure 31: Wafer w/ Exposed Silicon ... 48
Figure 32: Exposed Silicon under Microscope ... 49
Figure 33: DRIE Chamber ... 50
Figure 34: Etching Process ... 50
Figure 35: Top Side Etched Wafer ... 52
Figure 36: Bottom Side Etched Wafer ... 53
Figure 37: I3 Isolator Complete ... 54
Figure 38: I9 Isolator Complete ... 55
Figure 39: Printed Isolator ... 56
Figure 40: FormLab's Form 2 Printer ... 56
Figure 41: Printed Isolator Complete ... 57
Figure 42: Laser Vibrometer Setup ... 58
Figure 43: Fixture on Shaker (Silicon Isolator) ... 59
Figure 44: Fixture Design ... 60
Figure 45: Isolator Fixture (Printed Isolator) ... 60
Figure 46: Fixture Assembled ... 61
Figure 47: I3 Undamped Results ... 62
Figure 48: I9 Undamped Results ... 63
Figure 49: I9 PDMS Results ... 64
Figure 50: I9 Sorbothane Results ... 65
Figure 51: I9 w/ Ni Mesh ... 66
Figure 52: Grey Printed Isolator Results ... 67
Figure 53: Tough Printed Isolator Result ... 68
Figure 54: Onyx Printed Isolator Result ... 69

# Introduction

This thesis is a collected record of the research, development, and testing efforts to mitigate the negative effects of mechanical vibration on MEMS sensors. Mechanical vibration can be seen in many dynamic and complex systems. Unless specified, vibration is usually an undesirable quality [1]. Mechanical vibration is particularly impactful for devices such as MEMS sensors under certain conditions. One notable condition is the presence of vibration components near the sensor's resonant frequency. Exciting the resonant frequency of a mechanical system will cause various components within the sensor to oscillate at a higher amplitude than the input vibration [2]. The high magnitude of movement could exceed the elastic deformation range of the component which would lead to permanent deformation [3].

To understand the function of the sensors and the inherent problem, extensive research was conducted. Specifically, information was gathered to characterize the elements within the system and their contribution to this phenomenon. The same research was then used to create a theoretical solution. This solution comes in the form of a mechanical isolator. To verify the theoretical solution, simulation work was conducted and models were finely adjusted to exhibit desirable performance. Once the simulations verified isolator function, fabrication was conducted. The various processes described in detail. Following development, the isolator prototypes were evaluated in simulated conditions. Although this research is ongoing, the latest prototypes offer immense capability to protect sensors form disruptive vibration.

## Mission Objection

The main objective of this study is to develop a passive mechanical isolator that will isolate a MEMS sensor from frequencies near and above the sensor's resonant frequency without impairing its normal operations.

## Background and Problem

Micro-electromechanical systems or MEMS are devices comprised of miniature electrical and mechanical components [4]. MEMS devices have a number of different applications and capabilities. For the interest of this study, the focus will be on MEMS accelerometers. Accelerometers are sensors that can detect and measure the translational acceleration of an object. This occurs by fixing the accelerometer to an object of interest and allowing dynamic mechanical elements (i.e. inertial masses) to affect instrumentation circuits within the sensor. This dynamic element is usually suspended by leaf springs attached to the body of the sensor. This method of effect can vary depending on the specifics of the sensor. A generalized setup can be seen in Figure 1 and was based on a known setup [5].

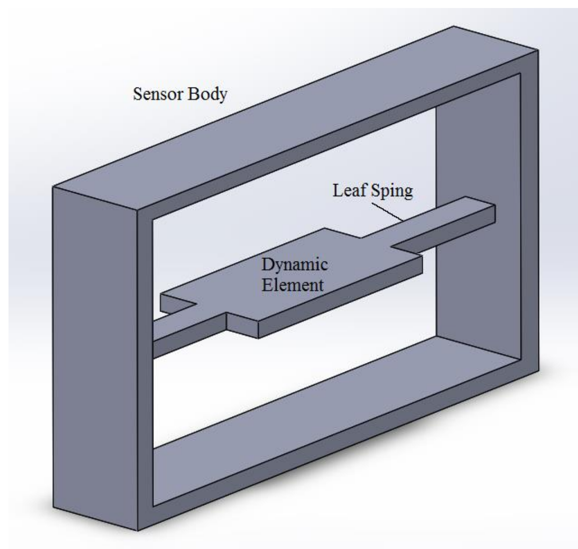


*Figure 1: Accelerometer*

A common approach to creating an accelerometer is attaching parallel conductive plates on a fixed point of the sensor and on the dynamic element. The incorporation of the plates into an electrical circuit creates a capacitor. Due to the inertial forces acting on the dynamic element during acceleration of the sensor, the displacement between the dynamic element and the fixed point within the sensor will change. This change in position will change the capacitance between the two parallel plates. Jacob Fraden's *Handbook of Modern Sensors* provides a fair example of an integrated circuit in which the output voltage is dependent on the displacement of the dynamic element relative to the body of the sensor. This circuit can be seen in Figure 2.

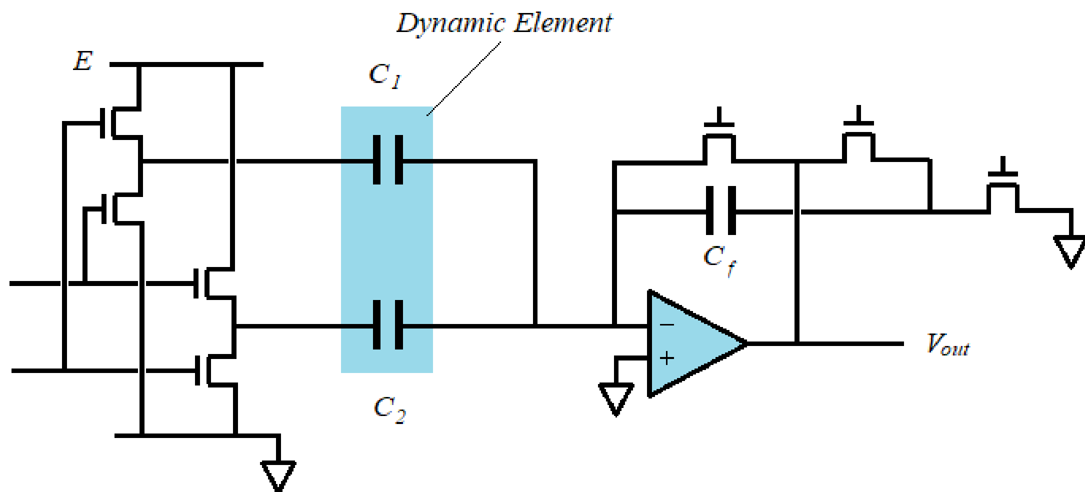


*Figure 2: Accelerometer Integrated Circuit*

In Fraden's rendition, a second pair of capacitive plates are utilized. This second pair, $C_2$, are placed on the opposite side of the dynamical element and body. The capacitance value of the second pair should be similar to the first pair with a 180 degree phase shift change. As seen in Equation 1, the output voltage is proportional to the capacitive difference between the parallel plate pairs [6].

$$V_{out} = 2E\frac{C_1 - C_2}{C_f} \quad \text{Eq1}$$

The issue with having physical components in a sensor is that the function of the sensor is more vulnerable to physical factors. One such factor is mechanical vibration. In most cases, the sensor and the dynamic element will oscillate near the same amplitude as the sensor's body and function normally. An issue arises when the vibration approaches the resonant frequency of the sensor and the system is underdamped. Under observation, the dynamic element will oscillate at a higher amplitude than the body of the sensor at the resonant frequency. Any large difference between the dynamic element and the body would be problematic as the output signal is no longer proportional to the actual vibration input. This will cause inaccurate information to be input into the system. Another issue is the likelihood that components will move beyond their intended range and plastically deform or catastrophically fail. Plastic deformation is a permanent damage to the components and because the sensor relies on the components, the sensor is effectively unusable.

To understand this phenomenon and to derive a possible solution, the system was broken down theoretically and reclassified into quantifiable terms. The accelerometer is analogous to a based excitation model as seen in Figure 3. The mass, m, represents the suspended dynamic element within the sensor and the spring and damper elements represent the suspension system of the dynamic element. The displacement of the mass is represented as the x component and the displacement of the frame is represented as the y component. This model is known as a base excitation model due to the inclusion of an oscillating base (e.g. input vibration). Any change in the ratio between x and y is regarded as a gain of the system, which is ultimately what needs to be defined.

m = dynamic element

k = spring constant

b = damping coefficient

x = dynamic element displacement

y = sensor body displacement

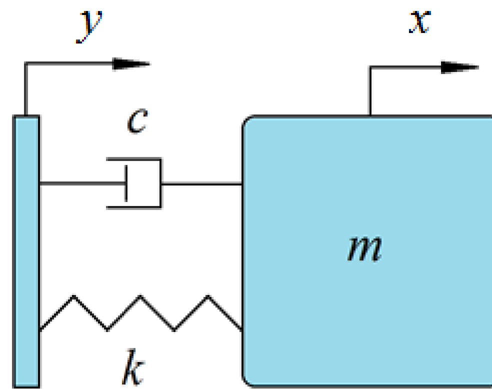


*Figure 3: Base Excitation Model*

The first step in finding the gain of the system was generating a single equation that can describe the motions of the dynamic element. This single equation is called the equation of motion. To begin the equation of motion, one must start with a fundamental idea of physics. That idea is Newton's second law of motion.

$$F = ma \qquad \text{Eq 2}$$

F = force

m = mass

a = acceleration

The next step is to find all of the forces acting on the dynamic element. With the suspension system being the sole interface within the dynamic element, the sum of the forces are the damping and spring forces of the suspension system.

$$\Sigma F = F_{damper} + F_{spring} \qquad \text{Eq 3}$$

To derive the equation of motion, the forces will need to be broken down into their dependent variables. The spring force is generated by a displacement difference and the damper force is generated by a displacement over time or velocity. The forces of each mechanical property are described in the equations below:

$$F_{spring} = k(y - x) \qquad \text{Eq 4}$$

$$F_{damper} = b(\dot{y} - \dot{x}) \qquad \text{Eq 5}$$

The equation of motion for the system can now be derived using the given information. Because the sum of forces is focused around the dynamic element, the acceleration of the element will be described as ‘ẍ’

$$\Sigma F = F_{damper} + F_{spring}$$

$$m\ddot{x} = b(\dot{y} - \dot{x}) + k(y - x) \qquad \text{(Equation of motion)}$$

This equation of motion describes the motion of the dynamic element. Many of the elements from the base excitation model are still present in the equation such as mass, m, spring constant, k, and damping coefficient, b. New components include the velocity of the excited base, $\dot{y}$ and the velocity of the mass, $\dot{x}$. The next step is to use this equation to find the expression for the ratio between the input displacement and the displacement of the dynamic element (i.e. the output). This expression is known as the transfer function of the system. First, the variables of the equation of motion are separated and rearranged into the following second order differential equation.

$$m\ddot{x} + b\dot{x} + \ kx = b\dot{y} + ky \qquad \text{Eq 7}$$

Second, the equation is transformed using the Laplace transform method. Initial conditions are assumed to be zero.

$$X(s)(ms^2 + bs + \ k) = Y(s)(bs + k) \qquad \text{Eq 8}$$

The final step is to solve for X(s)/Y(s).

$$\frac{X(s)}{Y(s)} = \frac{bs+k}{ms^2+bs+\ k} \qquad \text{Eq 9}$$

This transfer function is known as the displacement transmissibly and it can be used to understand the effect of the base movement of the dynamic element. The dynamic element, however, is in the s domain and will need to be converted to X/Y in order to obtain a system gain profile of the response across a range of frequencies. This conversion will need a few new items. The first item is the frequency of oscillation of the free response. The free response of the system is the part of the response that is dependent on the initial conditions, m, k, and b. This is also known as the natural frequency of the system or damped natural frequency if $b \neq 0$ [7]. To find the natural frequency of the system, one must solve for s in the denominator of the transfer function or the roots of the system. This is done using the quadratic formula.

$$ms^2 + bs + \ k = 0 \qquad \text{Eq 10}$$

$$s = \frac{-b \pm \sqrt{b^2 - 4mk}}{2m} = -A \pm Bj \qquad \text{Eq 11}$$

Note that the roots are assumed as complex. Breaking the root expression into real and complex parts yields:

$$A = -\frac{b}{2m} \qquad B = \sqrt{\frac{k}{m} - \left(\frac{b}{2m}\right)^2} \qquad \text{Eq 12, 13}$$

Due to the inclusion of all initial conditions, B is recognized as the damped natural frequency, $w_d$, of the system. If b is set to zero then the expression turns into the natural frequency, $w_n$.

$$w_d = \sqrt{\frac{k}{m} - \left(\frac{b}{2m}\right)^2} \qquad w_n = \sqrt{\frac{k}{m}} \qquad \text{Eq 14, 15}$$

With the damped natural frequency determined, the next step was to solve for the damping ratio, ζ. The damping ratio is described as the damping coefficient of the critical damping coefficient. The damping coefficient is given initially, but the critical damping coefficient needs to be derived. When a system is critically damped, the damped natural frequency is brought down to zero. Setting the damped natural frequency expression to zero will allow one to solve for the critical damping coefficient. [7]

$$w_d = 0 = \sqrt{\frac{k}{m} - \left(\frac{b}{2m}\right)^2} \qquad \text{Eq 16}$$

$$b_{critical} = 2\sqrt{mk} \qquad \text{Eq 17}$$

With the critical damping coefficient derived, the damping ratio can be found. The damping ratio is shown in the equation below.

$$\zeta = \frac{b}{b_{critical}} = \frac{b}{2\sqrt{mk}} \qquad \text{Eq 18}$$

With the necessary items collected, the final steps of finding the X/Y function is to substitute the items into the existing transfer function and substituting the s domain variable with *jw*. Note that *j* is equal to $\sqrt{-1}$.

$$\frac{X(s)}{Y(s)} = \frac{bs+k}{ms^2+bs+k} = \frac{(\frac{c}{m})s+k/m}{s^2+(\frac{c}{m})s+k/m} = \frac{2\zeta w_n s+w_n{}^2}{s^2+2\zeta w_n s+w_n{}^2} \qquad \text{Eq 19}$$

$$s \rightarrow jw$$

$$\frac{X(jw)}{Y(jw)} == \frac{2\zeta w_n jw+w_n{}^2}{-w^2+2\zeta w_n jw+w_n{}^2} \qquad \text{Eq 20}$$

Dividing the numerator and denominator by $w_n^2$ yields

$$\frac{X(jw/w_n)}{Y(jw/w_n)} = \frac{2\zeta(w/w_n)j+1}{1-w^2/w_n{}^2+2\zeta(w/w_n)j} \qquad \text{Eq 21}$$

Substituting $w/w_n$ for frequency ratio r yields

$$\frac{X(jr)}{Y(jr)} = \frac{2\zeta rj+1}{1-r^2+2\zeta rj} \qquad \text{Eq 22}$$

Eliminating *j* via direct magnitude of the expression will produce X(w)/Y(w) or X/Y.

$$\left|\frac{X(jr)}{Y(jr)}\right| = \frac{X(r)}{Y(r)} = \sqrt{\frac{4\zeta^2r^2+1}{(1-r^2)^2+4\zeta^2r^2}} \qquad \text{Eq 23}$$

With the transfer function of the system described, the gain profile across a range of frequencies can be found. When given the typical initial property values, the expression is able to produce a system gain profile known as the displacement transmissibility. This profile can be seen in Figure 4. Note the x axis is based on the frequency ratio and 1 is equivalent to the applied frequency set to the damped natural frequency of the system.

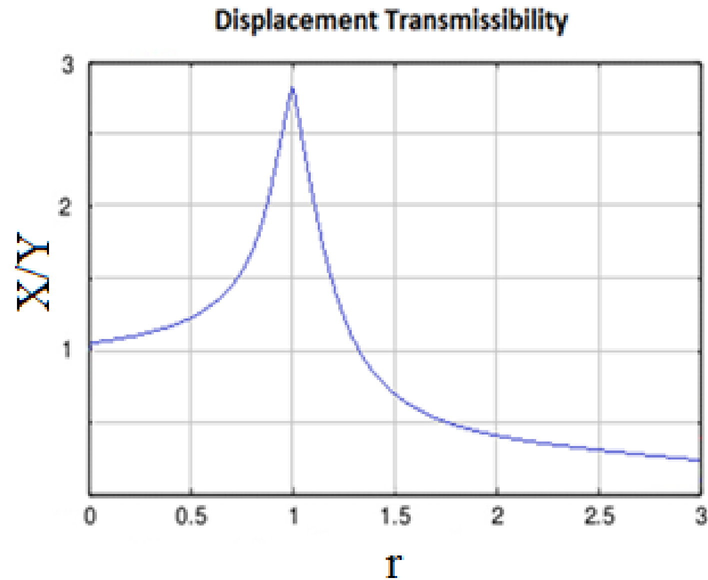


*Figure 4* :Gain vs Frequency Ratio Plot

Based on Figure 4, one could see how the system behaves. Below the natural frequency, the gain stays close to one or unity. As the applied frequency comes closer to the natural frequency the gain increases. At r = 1, the gain is at its absolute maximum. Following the natural frequency, the gain begins to drop rapidly. At a point past the natural frequency, the gain was low enough to no longer exhibit detectable excitement at such frequency. This is known as frequency attenuation. The theoretical gain profile is analogous to what is observed in real world instances. Unity between the base and dynamic element of the accelerometer remains constant below the natural frequency. The gain spikes once the natural frequency of the system is excited and the frequencies beyond the natural frequency attenuate. This spike is the gain in the original problem. As mentioned previously, this gain means high displacement of components within the affected sensors and could lead to plastic deformation or catastrophic damage.

## Theoretical solution

With the initial problem defined, the next step is to create a solution. One solution is the use of mechanical isolators. As the name implies, isolators alleviate this problem by isolating the sensor from vibrations above its natural frequency. Isolation usually involves reducing the amplitude of frequencies above the natural frequency. The presence of the frequencies will always be there; however, the amplitude is low enough so that the effects are minimized. There are two methods of accomplishing mechanical isolation. The first method is placing the sensor on top of a mechanical actuator and forcing the actuator to oscillate out of phase to the sensor's natural frequency. Out of phase vibration will effectively cancel the frequency's amplitude. This method is known as active vibration control.

The more ubiquitous variant of active system is electrostatic actuators. Electrostatic actuator are comprised of two parallel conductive plates with one plate fixed and the other suspended by a flexibility support. The configuration can be seen in Figure 5. A voltage difference is induced on the plates which causes an attractive force between the plates. Conditioning the episodes of pull and release into a periodic sequence will create an oscillation of the suspended plate. The suspended plate serves as the MEMS device platform [8]. In terms of raw performance, active vibration control is the most effective measure in isolating the sensor; however, this control system adds size, complexity, and energy to the sensor module and may not be a viable option with given application parameters [9].

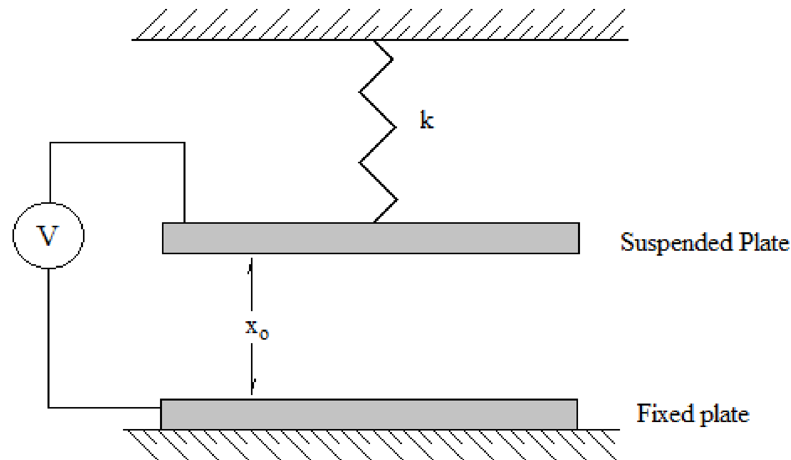


*Figure 5: Electrostatic Actuator*

The second isolation method is known as passive vibration control. Passive vibration control uses its structural qualities to attenuate the amplitude at a certain frequency and above. Passive isolation accomplishes this by relying on its mechanical properties to trigger its own natural frequency. At first it may seem counterintuitive to introduce a second natural frequency into the system; however, this is a critical component to passive isolation. As mentioned before, when a vibrating system is approaching its natural frequency, components of the system will oscillate at a higher amplitude compared to the source vibration until reaching the highest ratio at the natural frequency. Once past the point of natural frequency, the ratio will quickly decrease and experience frequency attenuation.

Deploying a sensor as the dynamic element of a base excitation system can create the passive isolators. By setting the isolator's natural frequency sufficiently below the natural frequency of the sensor, the isolator's natural frequency will come first and the attenuation that follows will overlap the sensor's natural frequency. This overlay will effectively reduce the sensor's natural frequency amplitude and minimize its effect on the sensor. This approach of

cutting off high amplitudes can be observed in Bochoa Wang's research in isolation study against harmonic forces. In his research, it was found that applying adaptive frequency magnetic fields can reduce the energy flow into the system. [10] This concept is demonstrated in Figure 6 and Figure 7.

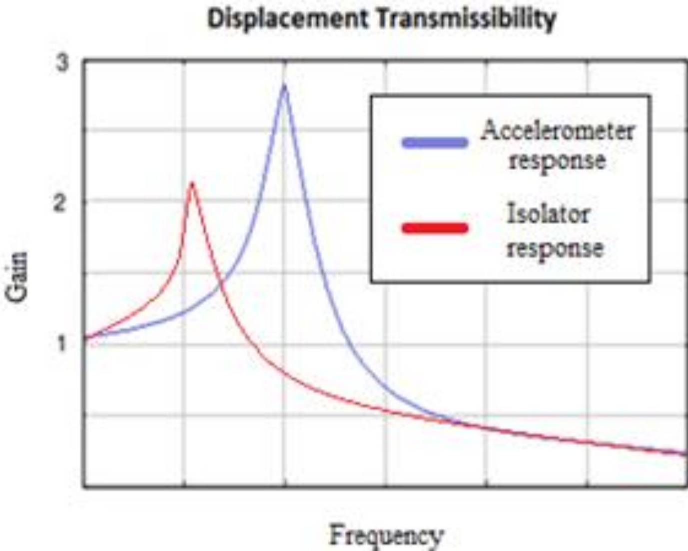


*Figure 6: Responses*

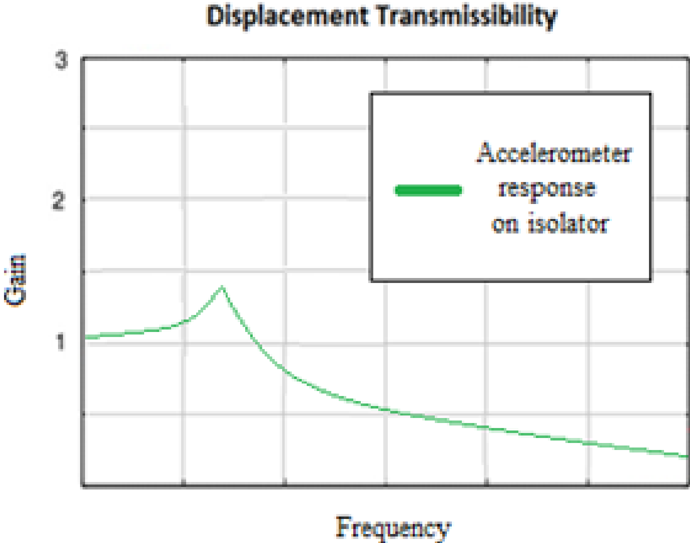


*Figure 7: Isolator Sum Response*

The conservative approach to creating an isolator with its own natural frequency is to mimic the general concept of devices known to have an excitable natural frequency. Based on the case of the accelerometer, the large mass suspended by several leaf springs seems to be a viable concept. As one can see in Figure 8, the upscaled dynamic element can serve as the platform for the accelerometer and the electrical traces that accompany it. The sensor and large dynamic element will serve as a single mass and the leaf springs of the isolator will serve as the spring and damper components. Note that an additional damping component is needed for some designs for added damping.

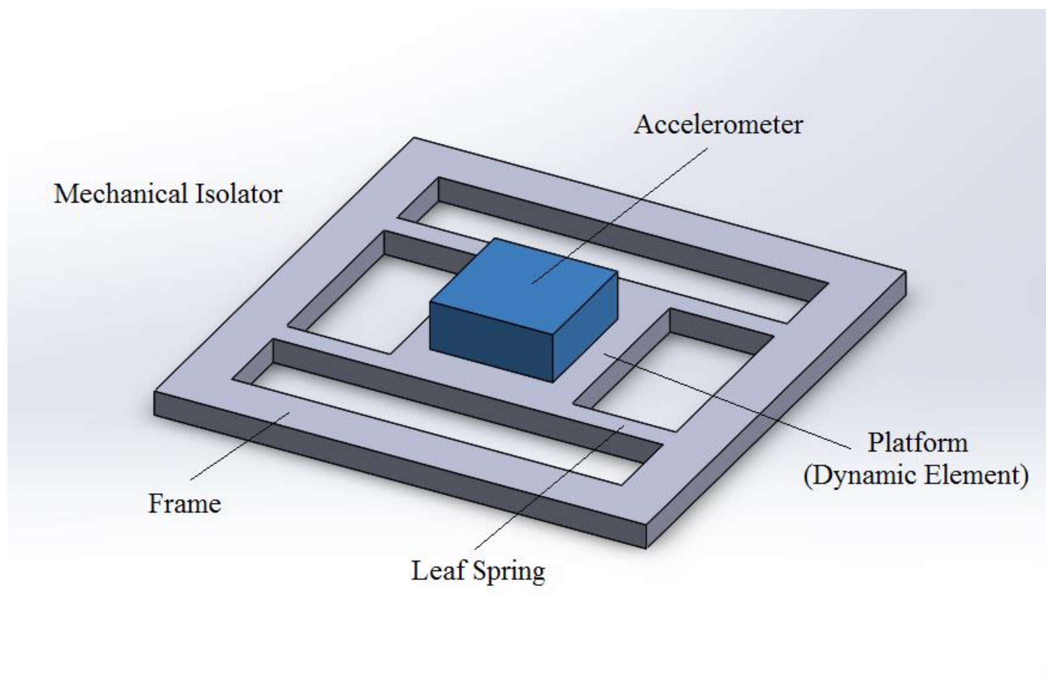


*Figure 8: Mechanical Isolator*

With the objective being to set the natural frequency and peak amplitude of the isolator below that of the accelerometer's several mechanical properties will need to be adjusted. Based on Equation 13, the natural frequency is dependent on the spring constant and the mass of the system;

however, this is not the complete case for the final response. Due to the damping element of the system, the appropriate expression for the system response is the damped natural frequency or resonant frequency. Components of the resonant frequency equation have already been determined in the previous section and the expression can be rewritten as:

$$w_{resonance} = w_n \sqrt{1 - 2\zeta^2} \quad \text{Eq 24}$$

$$w_{resonance} = w_n \sqrt{1 - 2(\frac{b}{b_{critical}})^2} \quad \text{Eq 25}$$

$$w_{resonance} = w_n \sqrt{1 - 2(\frac{b}{\sqrt{4mk}})^2} \quad \text{Eq 26}$$

Based on these expressions, the resonant frequencies can be set through the adjustment of the isolator's initial conditions. The second part of this objective was to adjust the peak amplitude of the resonant frequency. Although the peak of the isolator's response is not close to the natural frequency of the accelerometer, the high amplitude can still a pose danger to the sensor and its signal. A low amplitude is an important factor for the isolator's function. Based on Figure 4, the peak amplitude is dependent on the damping ratio [7]. The higher the ratio, the lower the peak; however, the attenuation after the peak will diminish. If the ratio is set to one or $b^2 = 4mk$, the gain across the frequency range would remain at unity. This occurrence is known as being critically damped and is not ideal for the function of the isolator. Setting the ratio below one will allow attenuation to occur.

## Parameters

With a clear understanding of how to theoretically solve this problem, the next stage was to design an isolator that follows the theoretical solution. The design has to follow a list of mission parameters set by the project sponsor. The parameters are as follows:

- The resonant frequency of the isolator must be near 1.0 kHz (no more than 1.5 kHz).
- The peak magnitude of the transmissibility curve of the isolator must be at or below 5.
- Isolator must be capable of hosting electrical traces.
- Isolator platform must be no less than 3.5 mm x 3.5 mm.
- Isolator footprint must be no greater than 12.5 mm x 12.5 mm.
- Isolator will also serve as the main housing for the sensor.

## Design

Given the parameters, there are two possible approaches to completing the mission objective. The two approaches are the construction of an isolator through traditional microfabrication and constructing it through additive manufacturing. The means of manufacture often dictate the final design, so an isolator design for each approach was developed. This section will provide a general overview of each approach and describe each isolator design

The isolator will serve as a package for the accelerometer and it is desirable to have the isolator as small as possible. This pursuit will make integration into other electronic systems more

viable. This microscale packaging is a difficult parameter to achieve; especially with features such as leaf springs. This type of device packaging is often reserved for a manufacturing process known as microfabrication. Microfabrication is the process of manufacturing physical objects in the sub millimeter domain [11]. The main application for microfabrication is the development of integrated-circuit (IC) and micro-electromechanical systems (MEMS). The dominant building material for microfabrication is silicon. Silicon is a semiconductor material with unique and useful characteristics. The most valuable quality of silicon, especially for IC, is the ability for its electrical properties to be modified through either doping or Ion implantation. [12] This quality allows for the fabrication of electronic components such as transistors to be realized in a silicon mass. Another quality is the precision of which silicon can be removed or etched. With delicate features such as leaf springs, high precision removal of material is very applicable to this study. Single crystal silicon usually comes as a disk called a wafer and is nearly a perfect crystal at the atomic level. [13] The fabrication process will be discussed in the fabrication section.

Silicon based isolators were designed based on the capability of microfabrication; specifically the capability of Auburn University's Woltosz Engineering Research Laboratory (WERL). The generation 3 isolator can be seen in Figure 9. The dimension of the overall footprint being a 7mm x 7mm square, 600 micrometers thick. The isolator features 16 leaf springs that support the central platform. The leaf springs are folded along the horizontal plan to allow for additional spring length inside the limit space. The thickness of the spring is predetermined by the thickness of the device layer of the SOI wafer which is 100 microns.

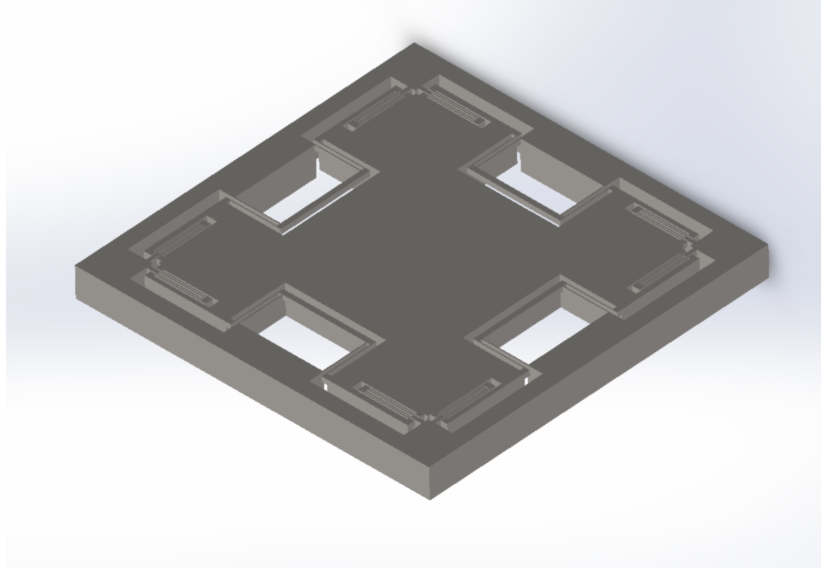

*Figure 9: I3 Isolator*

The next silicon isolator is the I9 and it can be seen in Figure 10. The dimension of its overall footprint being a 9mm x 9mm square, 600 micrometers thick. The I9 is the next evolutionary step from the I3. The design progression was an attempt to make the isolator more robust and house a larger selection of devices.

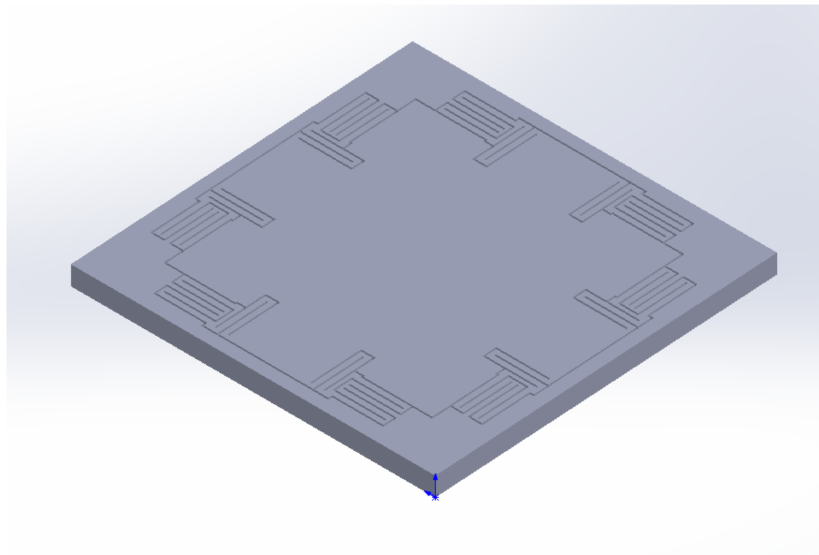

*Figure 10: I9 Isolator*

Each of the silicon designs were tuned to have a resonant frequency below 1.0 kHz. This is because silicon is nearly perfectly elastic with low thermoelastic damping [14]. Low damping translates to high peak transmissibility which is not desirable. Based on Equation 24, adding a damping component to the system to lower the peak will in turn decrease the resonant frequency. The lower the inherent resonant frequency will ensure that the final resonant frequency, including additional damping, will be within the parameters.

## Additive Manufacturing

Additive manufacturing or 3D printing is the process of constructing physical objects from digital information. The process typically involves stacking successive layers of material and bonding them together into a single homogeneous piece [15]. 3D printing was first introduced by Dr. Hideo Kodama of the Nagoya Municipal Industrial Research Institute in the early 1980's [16]. His publication "Automatic Method for Fabricating a Three-Dimensional Plastic Model with Photo hardening Polymer" described his process of exposing thin layers of photo-hardening plastic to UV radiation and stacking each layer to form a single mass. Shortly after Kodama's publication, other inventers developed and patented similar technologies.

Thirty years after Kodama publication, 3D printing had grown into a multibillion-dollar industry [17]. With many of the original patents expired by the mid 2000's, entry into the market became substantially easier for both producers and consumers. Initially, 3D printing was a subpar choice compared to other fabrication methods such as subtractive manufacturing and casting. The technology had several limitations including precise material placement, reliability of bonded layers, and quality of printable material [18]. These limitations regulated 3D printing to less demanding applications such as crafting and conceptual modeling. With the technology within public domain and a growing market, these limitations were short lived.

The latest generation of 3D printing has shown impressive capabilities. Resolution of prints are now in single microns and material such as ceramic and metals have become printable [19]. Other materials, advancements, and prospects in future applications can be seen in Vivek Baskaran's study "Current Applications and Future Perspectives of the Use of 3D Printing in Anatomical Training and Neurosurgery" [20]. This study is based off the idea of Baskaran's study and investigated the possibility of using 3D printing to create mechanical isolators.

The design of the printed isolator can be seen in Figure 11. As one can see, the design follows closely to the I9 design. The biggest deviation is the general proportions. The micro fabricated isolator maintains an overall footprint of 9 x 9 mm while the printed isolator was up scaled to 25 x 25 mm. Initial attempts were made to print a 9 x 9 mm isolator; however, the resolution of the printer would not allow for such small feature sizes.

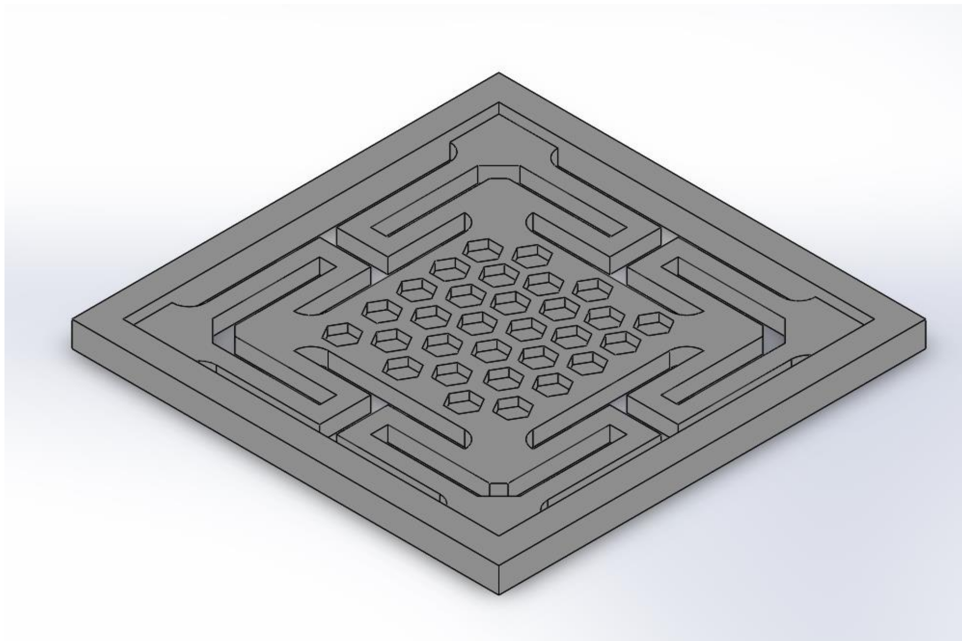

*Figure 11: Printed Isolator*

## Damping

As previously stated, silicon isolators will need damping elements in order to lower the peak magnitude of their transmissibility profile. This was accomplished by attaching damping material to the bottom side of the isolator platform and fixing the material to the excited base. An illustration of this can be seen in Figure 12. The theory behind this approach would be energy loss through the damping material during system oscillation [27]. The damping materials in this study were solid objects that can reform to their original geometries after moderate compression. This ability to reform is an indication that the material bears a spring quality. This spring quality will add to the net spring constant of the system once the damping material is integrated. This increase in spring constant will increase the resonant frequency.

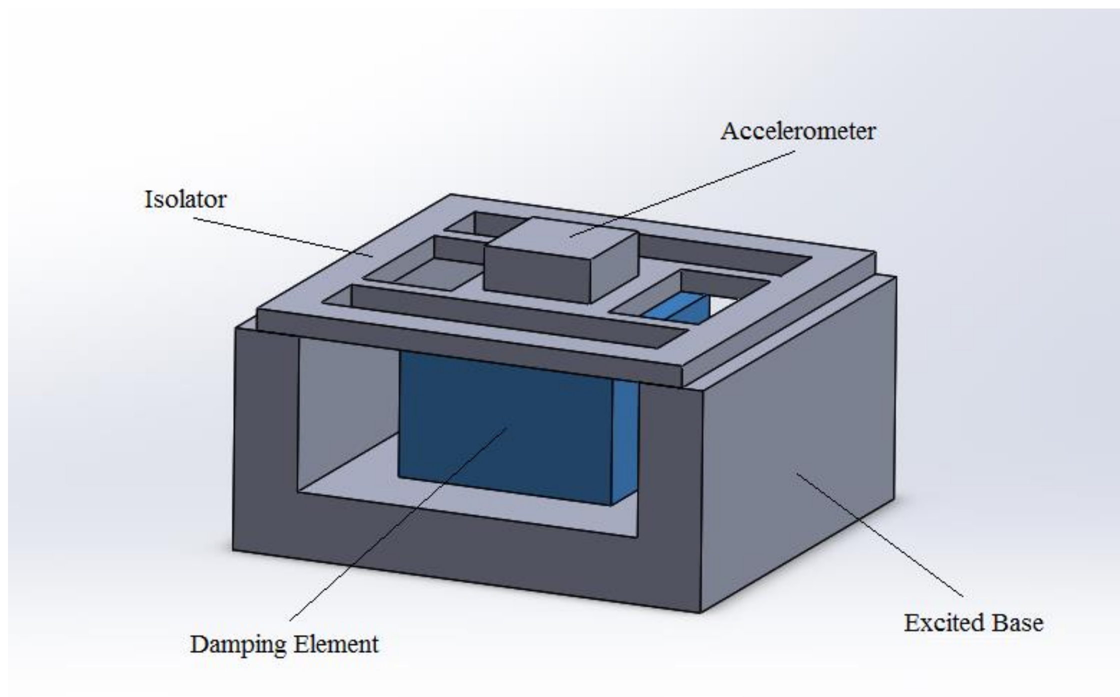


*Figure 12: Isolator w/ Damping Element*

Several materials were examined over the duration of the study. These materials include copper mesh, nickel mesh, PDMS, and Sorbothane. Copper and Nickel microfibrous mesh consisting of interwoven strands of copper and nickel. Individual strands measure on the order of tens of microns in diameter. Several combinations of Cu and Ni mesh thicknesses and test fixture cavity depths were tried in this study. Polydimethylsiloxane (PDMS) is an organosilicon polymer used in a variety of applications ranging from micro fluidics to additives in food and cosmetics. The PDMS used for testing was Sylgard 184, a Dow Corning Corporation product. Preparation of PDMS requires the mixing of a 10:1 PDMS: curing agent ratio. Sorbothane is a proprietary, visco-elastic polymer commonly used in applications ranging from acoustic vibration damping to orthotics.

## Simulation

Simulations are an important tool to have for any development; as it can be used to estimate the behavior of a prototype without an enormous amount of time and resource. This section will focus on the simulation aspect of each design. The physical engine used for this study was SolidWorks Education Edition 2018 SP5.0. Each isolator renders as a .prt file. The renderings can be seen in Figures 9, 10, and 11. Once the isolators were rendered, the next step was to start a Finite Element Analysis (FEA) study. This begins with creating a new assembly file and placing a 3 x 3 x 4.5 mm aluminum block at the center of the isolator platforms. The aluminum cube will simulate a typical attached accelerometer with a mass of 0.8 grams. The assemblies can be seen in Figures 13, 14 and 15.

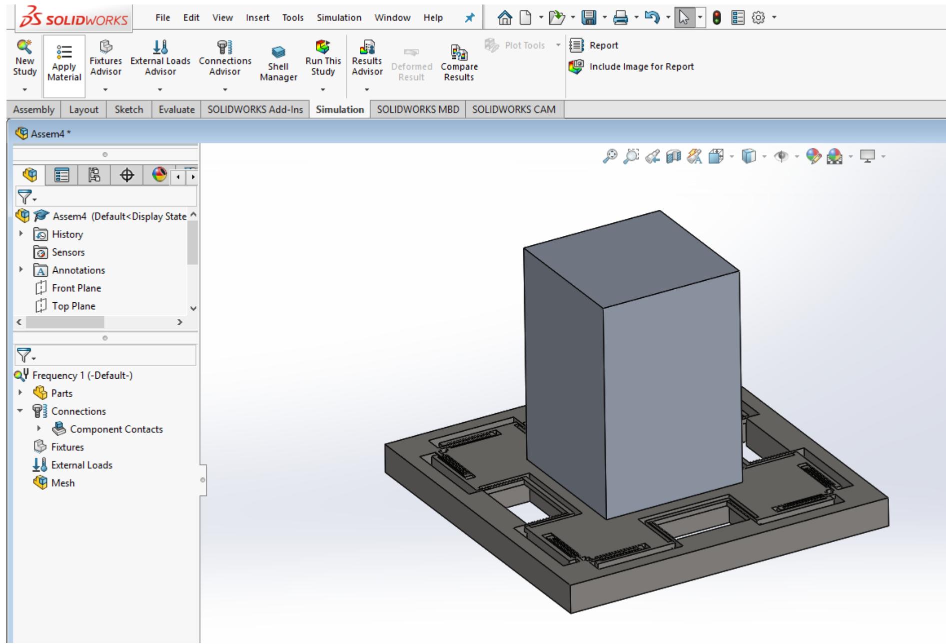


*Figure 13: I3 w/ Proof Mass*

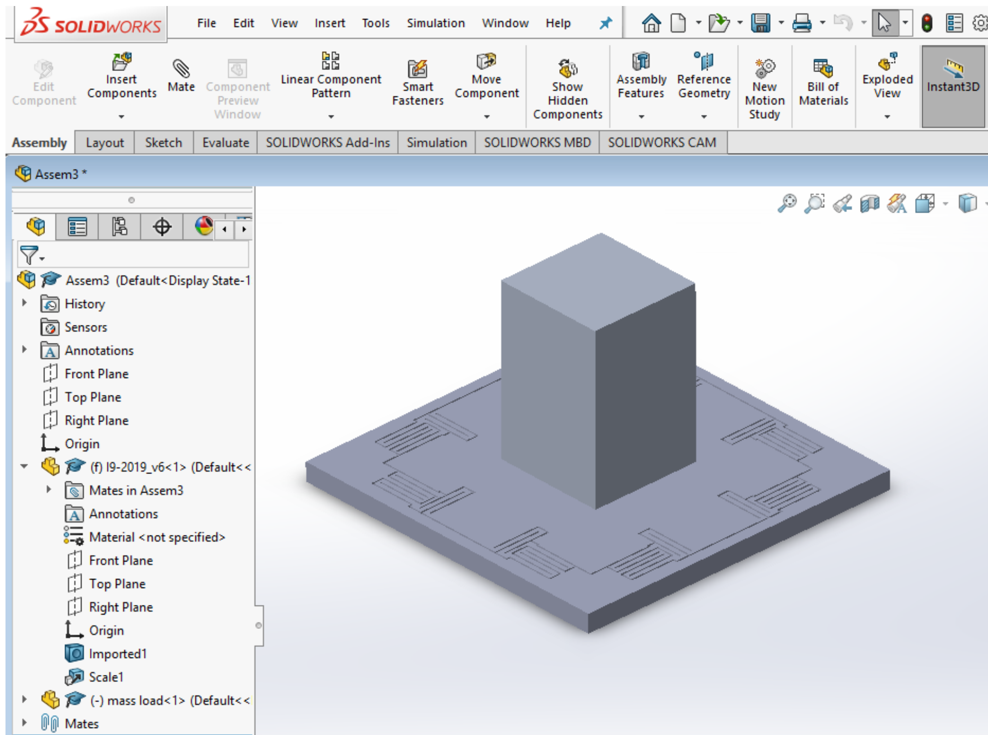


*Figure 14: I9 w/ Proof Mass*

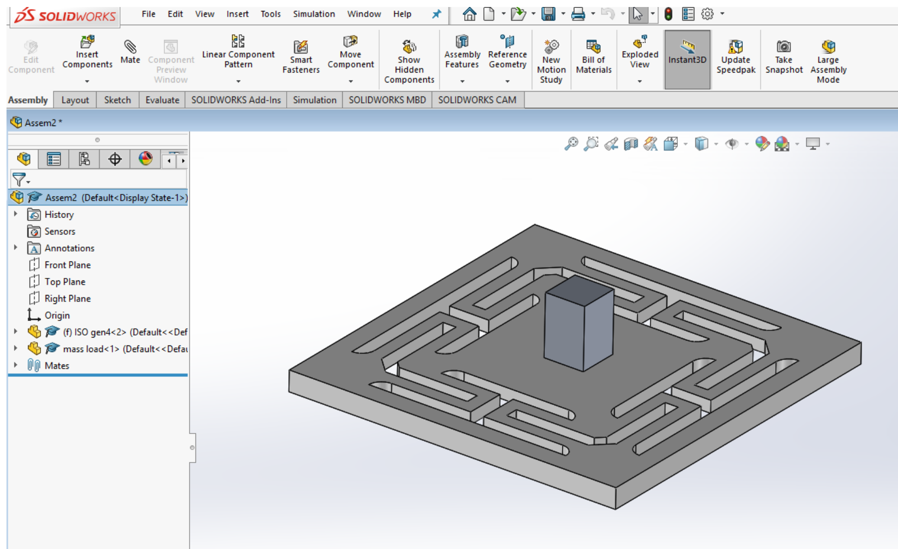


*Figure 15: Printed Isolator w/ Proof Mass*

With the assembly files ready, the next step was to instruct SolidWorks to begin a new study. This was done by clicking on the simulation tab and selecting "New Study." The Frequency option was selected under General Simulation then the green checkmark was selected. The next step was to establish the parameters.

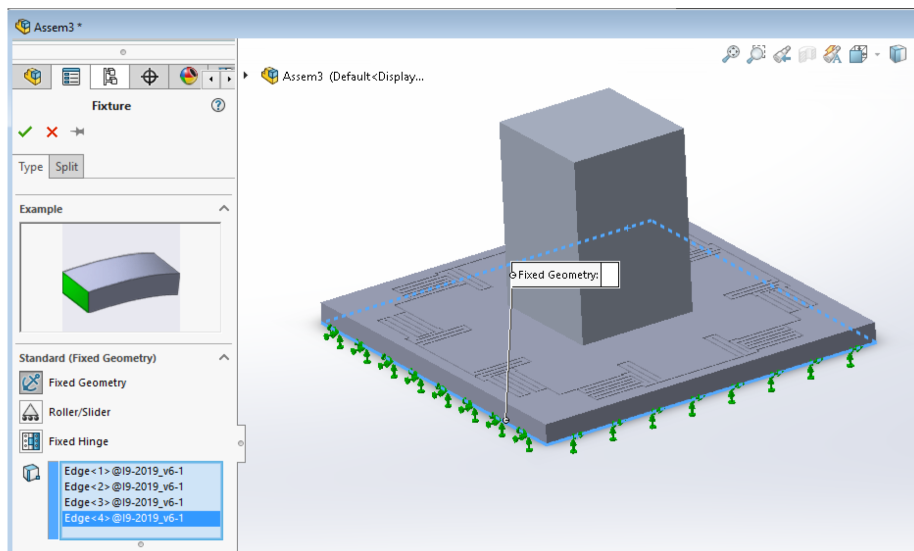


*Figure 16: FEA Boundaries Setup*

The first parameter was fixing the frame. Fixing the frame was accomplished by selection of the arrow under the “Fixture Advisor” tab and selecting "Fixed Geometry." The next step was to select all or near the points that were needed to be fixed. An example of this can be seen in Figure 16. After fixing the frames, the next parameter was to assign each component a material. For the micro fabricated isolators, the SolidWork’s built-in material ‘silicon’ was used. The properties of the silicon can be seen in Figure 17. The aluminum block was assigned to SolidWork’s “1060 Alloy” material.

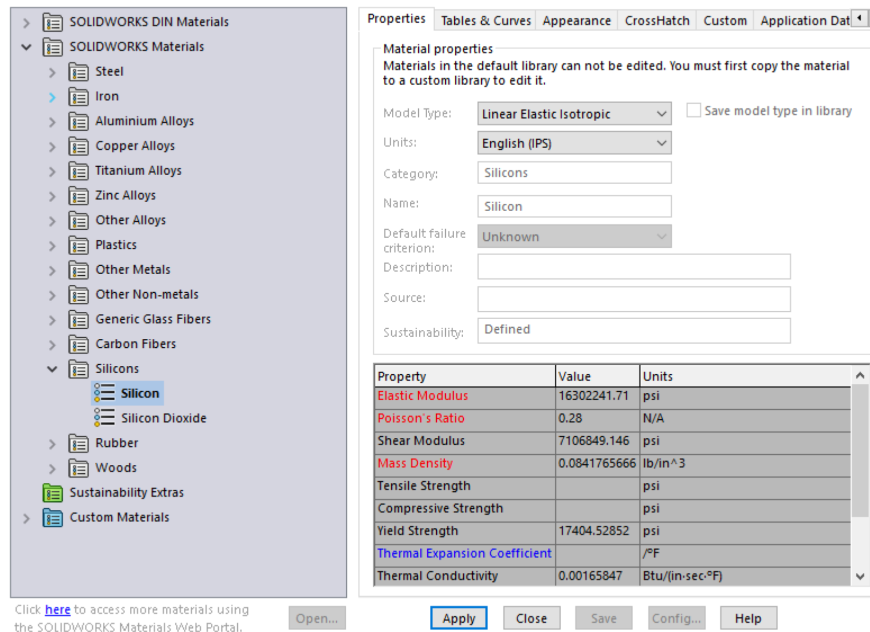


*Figure 17: FEA Silicon Material Properties*

For the 3D printed isolator, a custom material had to be made. The material was based on FormLab’s FLGPGR04 Resin. The properties were sourced from Formlab’s online datasheet [21]. The Properties of the resin can be seen in Figure 18.

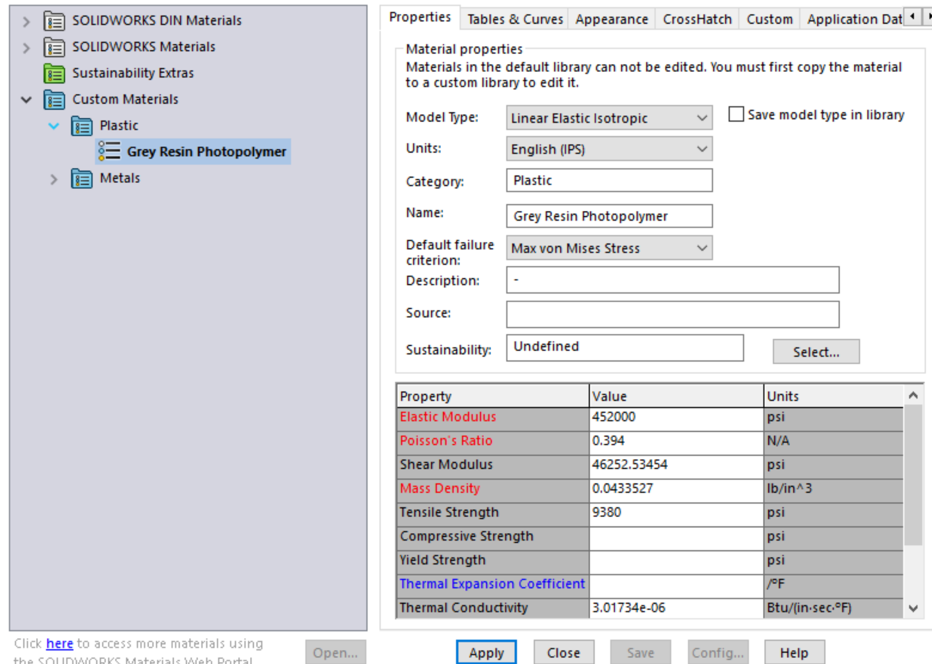


*Figure 18: FEA Resin Material Properties*

With the parameters set, the final step was to execute the FEA study. This was done by going under the simulation tab once again and selecting “Run this Study.” The simulation took a couple of minutes to complete and the primary mode (Frequency 1) was displayed by default. This primary mode is the resonant frequency along the y axis of the assembly. Other modes will be available as well. These modes represent the resonant frequency of different axes and even rotations. These additional modes are the consequence of the high center of mass of the aluminum block. In real world conditions, the accelerometer’s center of mass will be lower and would not produce these modes. The simulation results of the isolators can be seen in Figures 19, 20, and 21.

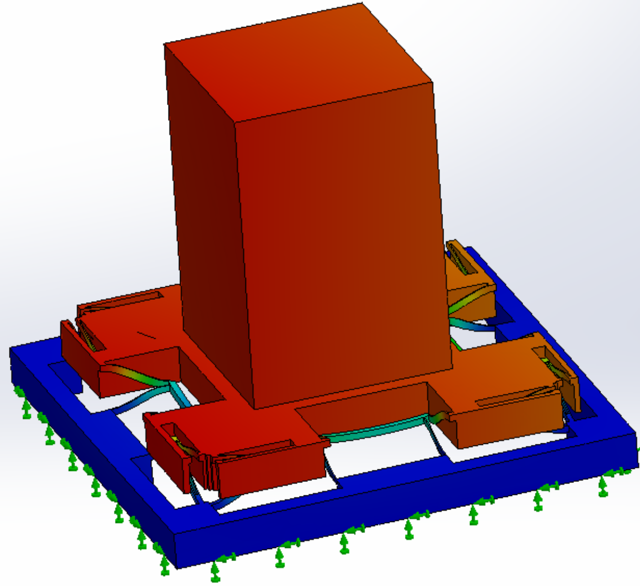


*Figure 19:FEA I3 Results*

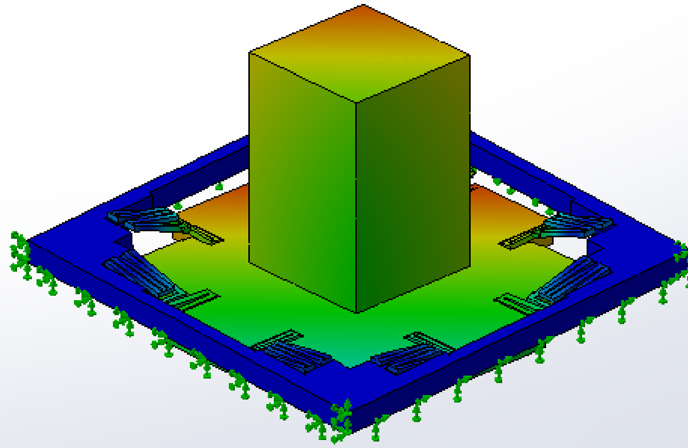


*Figure 20:FEA I9 Results*

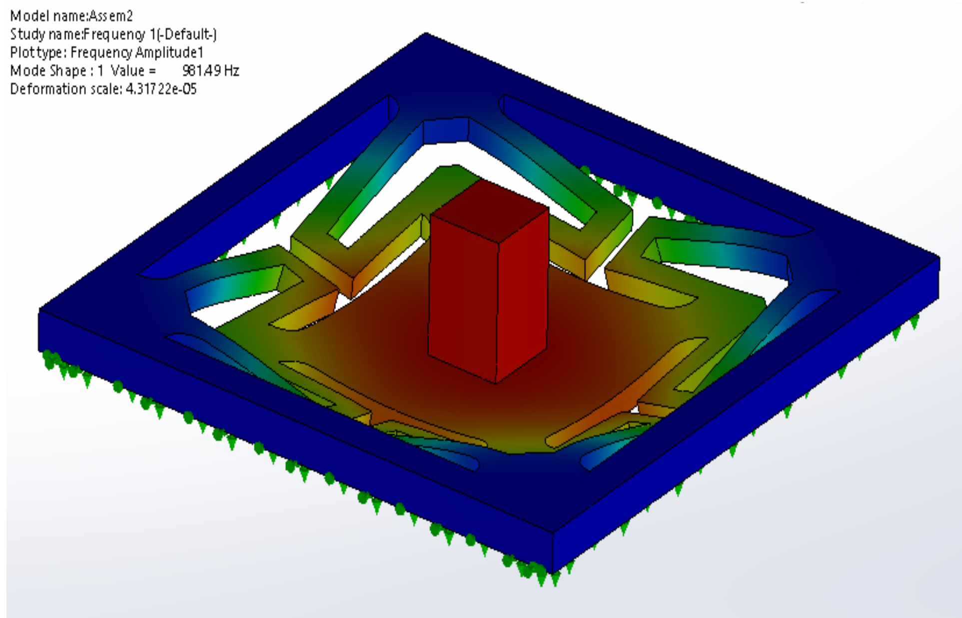


*Figure 21:FEA Printed Isolator Results*

As previously mentioned, the micro fabricated isolators intentionally have lower resonant frequencies than the 1.0 kHz target value. This will be to offset the additional damping element. The increase in damping will lower the peak transmissibility of the isolator but will increase the resonant frequency.

## Fabrication

Fabrication is a critical point in the development efforts of any project. Prior to existing in a real environment, ideas and the research behind them cannot extend outside the domain of theory. It is also one of the more vulnerable steps in any effort due to it bringing the mechanics of imperfection into the system. This is especially true for the development of isolators. The current design and high sensitivity to variables and the fabrication of these prototypes must be executed with extreme procession. This section will discuss the process for fabricating the two-concept design of this study. The literature will be split into two subsections—traditional micro fabrication and additive manufacturing. Each step in this subsection will include the equipment needed, instruction of how to use such equipment, and an illustration of the final product.

### Traditional Manufacturing:

The conservative method of fabricating MEMS devices is microelectronic fabrication. This process is most commonly used in the construction of integrated circuits (ICs). Microelectronic fabrications have many, and sometimes complex, steps. To help understand this process, Figure 22 illustrates the general fabrication flow. Note that each of the illustrations are a side view of the product of each step. The following section will present the instructions for each step. The silicon based isolator, I9, will serve as an example for each step.

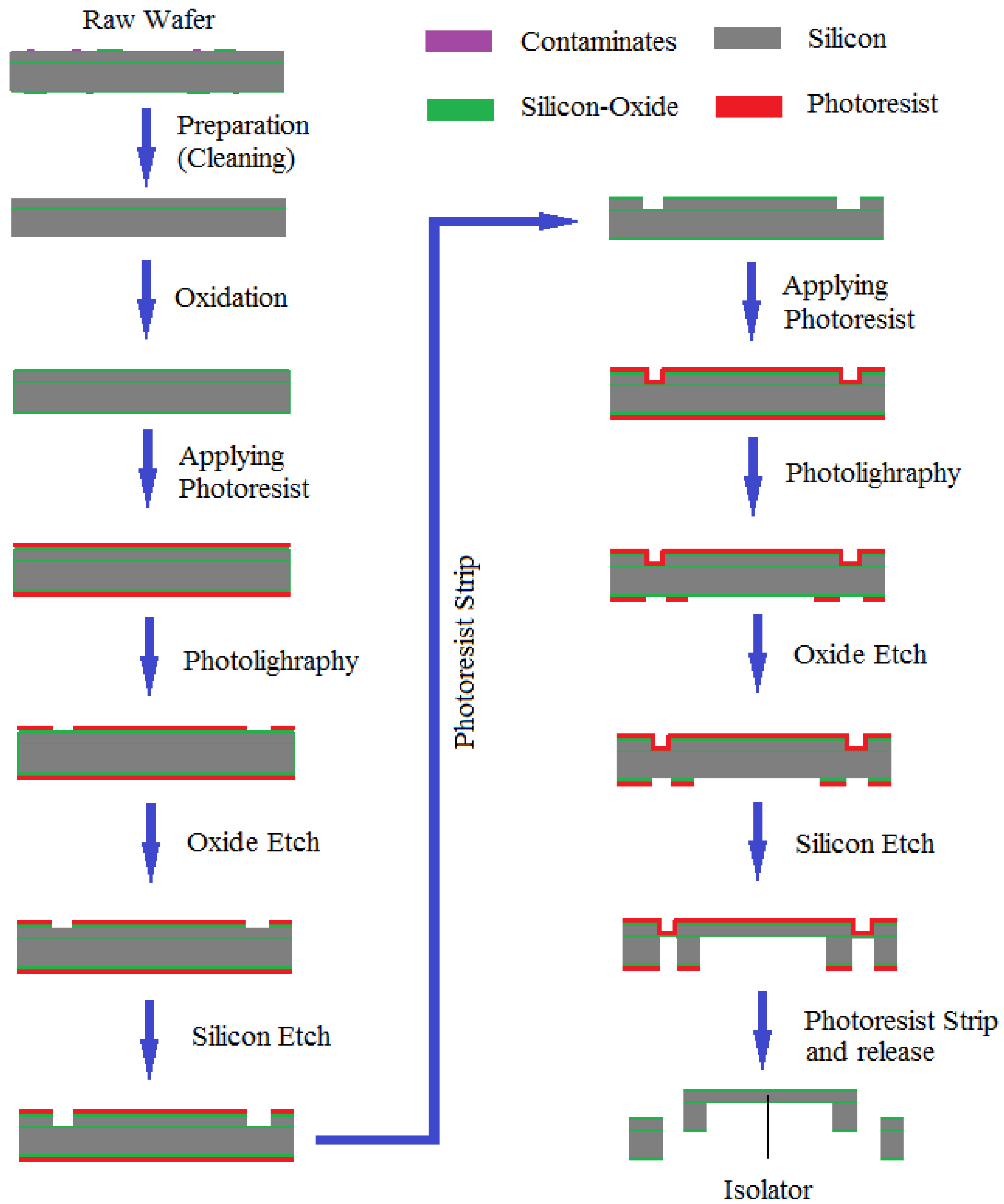


*Figure 22: Fabrication Process Flow*

Raw Material

The most common material for microelectronic fabrication is silicon because it is an ideal groundwork to build from. Silicon is a semi-conductor and its electric properties can be modified to either allow or restrict electrical flow. This is possible with the implantation of certain atoms into the material by either ion implantation or diffusion [13]. One quality that is critical for the study is the mechanical properties of silicon. Silicon is nearly perfectly elastic, and its yield strength is near the point of fracture [14]. This means that the strain and potential deformation creep is not a significant factor in the long-term operation of the material [22]. This is a very valuable quality because the leaf springs are very delicate and would not last long if degradation was a significant factor. Another quality that makes silicon a favorable base material is its resistance to change under temperature.

The thermal expansion coefficient (CTE) of silicon is 2.6*10^-6 m/(m*K) [23]. Compared to other materials, such as steel or aluminum, this coefficient is very low. Low CTE correlates to less expansion of material with varying temperature. This means less temperature actuated stress acting on the structure. This is very important for this study because pre-applied force is a major factor in the behavior of the isolator. Silicon for microelectronic fabrication typically comes in a disk-shaped profile called a wafer. The diameter of the wafer can be anywhere from 2.5 to 30 cm. For this study, four-inch wafers with crystal orientation <100> were used. A set of the silicon wafers can be seen below in Figure 23.

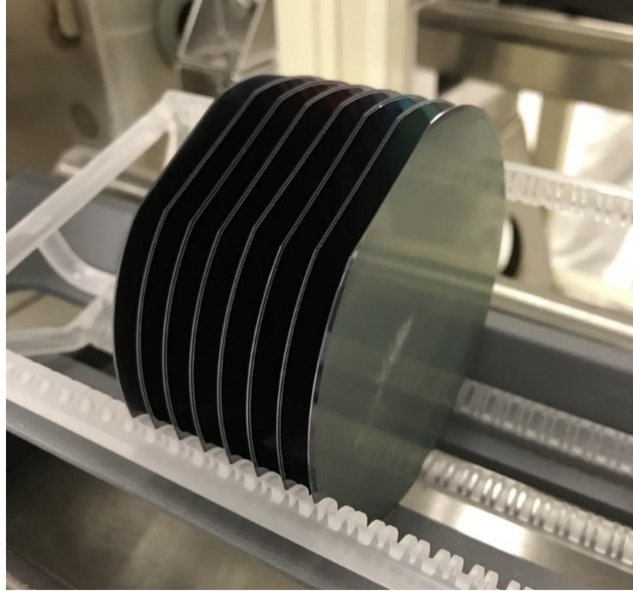

*Figure 23: Raw Silicon Wafer*

Due to the geometry of the isolator, a unique type of wafer was used. The wafer bears a silicon-oxide layer within it. A cut-away illustration can be seen in Figure 24. This type of silicon wafer is known as a silicon on insulation (SOI) and the silicon-oxide layer is regarded as the box layer. The box layer is only 1.5 microns thick and underneath approximately 100 microns of silicon. The silicon layer above the box layer is regarded as the device layer. This layer will become the top side of the isolator and springs. The 500 microns of silicon below the box layer is the handle layer and it will become the lower side of the isolator.

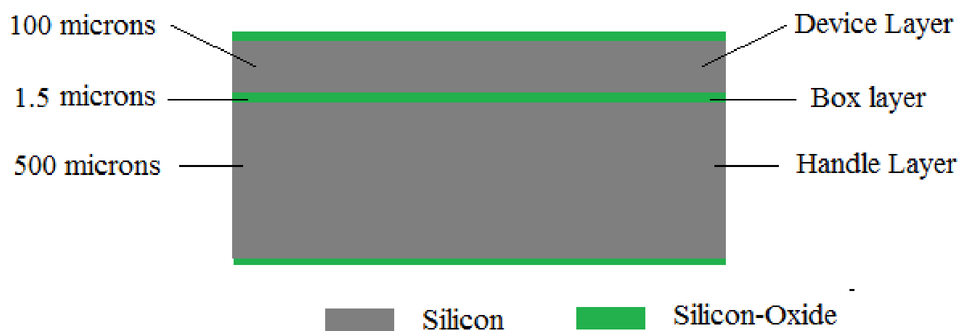


*Figure 24: SOI Wafer Material Profile*

## Preparation

Microelectronic fabrication is a sensitive collection of processes. The biggest threat to the fabrication process is the introduction of foreign particles. These particles can physically block the processing of certain areas and can damage the instruments. Due to how prone microfabrication is to foreign particles, special facilities are made to reduce the number of contaminants within the environment of the processes. These facilities are known as clean rooms. Clean rooms are, as the name implies, very clean spaces that constantly filter the air and keep the number of particles in the air below a desired level. The wafers have to be cleaned before processing can begin. Contaminants may be present from manufacturing and handling. The following process will describe the first cleaning required.

Cleaning begins with a wafer bath of a 50 to1 ratio of deionized (DI) water and hydrofluoric acid at an ambient temperature for thirty seconds. This step will strip native silicon oxide and allow for a fresh oxide build in the oxidation process. The second step is a 6:1:1 ratio of $H_2O$: HCl: $H_2O_2$ bath at 80° C for 10 minutes. This step is the main process that removes the contaminants. The final step is a DI $H_2O$ rinse and $N_2$ dry. This step will remove residue from the previous steps.

Oxidation

In a later process, silicon will be removed from the wafer. Some areas of the silicon wafer will be removed while other areas will remain. This selective removal of material is possible by creating a barrier that is resistant to the removal process and spares the silicon underneath. This barrier is silicon dioxide. This process of applying the layer is known as thermal oxidation. There are two types of oxidation processes: dry oxygen and 'wet' water vapor. The chemical reactions for each can be seen below:

Dry oxygen:

$$Si + O_2 \rightarrow SiO_2 \qquad \text{Eq 27}$$

Water Vapor:

$$Si + 2H_2O \rightarrow SiO_2 + 2H_2 \qquad \text{Eq 28}$$

These reactions are done inside an oven that can reach temperatures above 900° C. An oven and a tray are used to slide the wafer inside; this can be seen in Figure 26. For this study, a wet oxygen process was used. Since the oxide layer serves as a barrier for the etching process, the thickness of the layer is an important part to control. As the oxide layer is built on the wafer, the rate of oxidation slows down. The build-up rate is understood through Fick's first law of diffusion [13]. This law states that:

$$J = - D \, \partial N(x,t) / \partial x \qquad \text{Eq 29}$$

Where J is the particle flow per unit area equal to the particle concentration, $\partial N(x,t)$ , over area multiplied by a coefficient of diffusion, D. After analyzing Figure 3.3 of Jaeger's "Introduction to Microelectronic Fabrication," the oxygen particle flow, J, can be modified to

$$J = - D (N_i - N_o) / X_o \qquad \text{Eq 30}$$

Under this expression the particle flow is equal to the diffusion coefficient multiplied by the difference in silicon-dioxide concentration at the surface and the silicon dioxide-silicon interface, $(N_i - N_o)$ and divided by the oxide layer thickness, $X_o$ [13]. Because the objective is to grow a certain layer thickness on the wafer, a function for $X_o$ was needed. The rate of change of the layer thickness is equal to the particle flow divided by oxidizing molecules, M [13]. With this information, the difference of thickness change over time equals:

$$dX_o/dt = J/M = (DN_o/M)/(X_o + D/k_s), \qquad \text{Eq 30}$$

where $k_s$ is a constant rate of reaction at the interface. Setting the initial layer thickness to $X_i$ and isolating time yields:

$$t = X_o^2/B + X_o/(B/A) - \tau, \qquad \text{Eq 31}$$

where $A = 2D/k_s$, $B = 2DN_o/M$, and $\tau = X_i^2/B + X_i/(B/A)$. Isolating $X_o$ yields:

$$X_o = 0.5A[(1 + (4B/A^2)(t + \tau))^\wedge(1/2) - 1] \qquad \text{Eq 32}$$

The final step that will fully express $X_o$ is to find the coefficient, D. According to Jaeger, the mathematical model for this coefficient is:

$$D = D_o exp(-E_A/kT), \qquad \text{Eq 33}$$

Where T is the temperature for wet etching on a <100> wafer, Do = 9.70 x 107 microns/hr and $E_A$ = 2.05 eV. Taking the function for $X_o$ and assigning various conditions, such as temperature and time, this yields the profiles of oxide layer thickness. The profiles have been captured and illustrated in the Jauger's Thickness vs Time Figure 3.6. The Figure can be seen below as Figure 25.

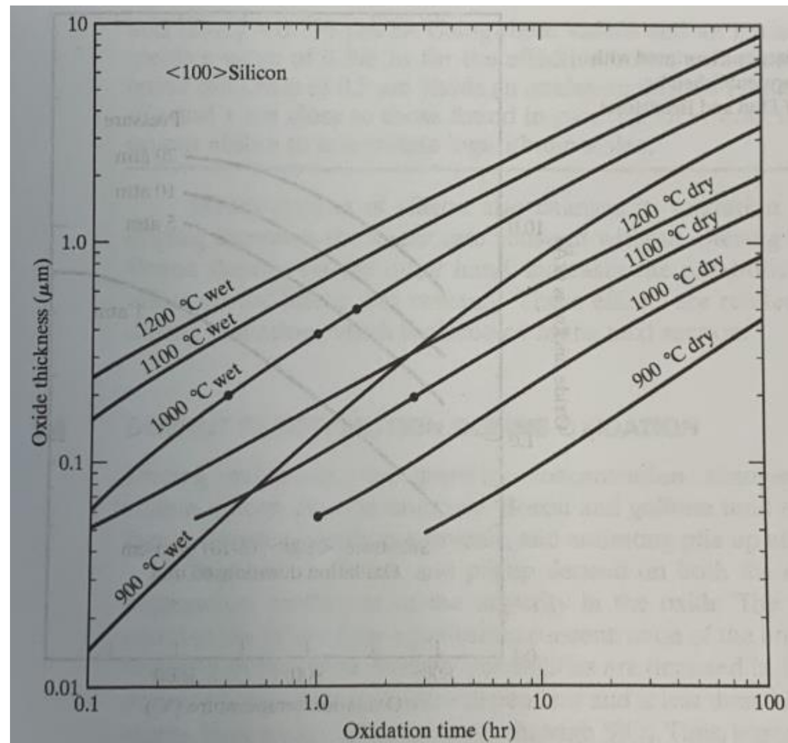


*Figure 25: Oxidation Thickness vs Time*

With a basic theoretical understanding of how silicon dioxide is grown on top of the wafer, the next step was to establish the desired thickness and execution plan for the oven. The desired thickness for the oxide layer is 0.5 microns. The achievable temperature for the oven is 1050° C. Based on these two items, the ideal time to expose the wafer to $H_2O$ is approximately 1.0 hour. Purging and temperature ramping are required for the oxidation process. This is to ensure survival and the quality of the wafer. The instruction for this process can be seen below:

Oxidation Instruction set:

1. Set oven to 900° C
2. Insert tray of wafers into the oven slowly (approximately 0.25 meters per minute)
3. Seal oven and wait for temperature recovery
4. Ramp temperature to 1050°C
5. Administer nitrogen, $N_2$, purge for 5 minutes
6. Administer oxygen, $O_2$, purge for 5 minutes
7. Administer Hydrogen, $H_2$, and oxygen into oven for 1.0 hour ($H_2O$ is formed)
8. Administer oxygen, $O_2$, purge for 5 minutes
9. Administer nitrogen, $N_2$, purge for 5 minutes
10. Ramp down to 900° C
11. Remove wafer tray out of oven slowly (approximately 0.25 meters per minute)

Following these instructions will produce a wafer with 0.5 microns thick oxide layers.

*Figure 26: Wafer Oven*

Applying Photoresist

With a layer of silicon oxide on the wafer, the next step was to select which area of the layer will remain for silicon etch resistance. This is done by a process known as photolithography. A thin layer of photoresist will be placed on top of the oxide layer and is partially removed with high resolution UV exposure. The remaining photoresist will protect the oxide layer when the oxide stripping process is administered to the wafer. This process begins with an acetone-isopropanol-methanol bath and $N_2$ blow dry. This will clean any residue left from the oxidation process. The next step was to place wafer into the oven for 10 minutes at 110° C. This step will ensure that there is no moisture on the wafer. The dry wafer was then placed into an enclosed container and exposed to 12 drops of HMDS for 10 minutes. The HMDS will aid on the boding between the wafer and photoresist.

The next step was to place the wafer on the head of a spinner as seen in Figure 27. Photoresist, known as AZ-9245, was poured onto the wafer. The wafer was then spun, which forced the photoresist to spread evenly across the wafer. The spinner followed a (1700/500/5/2200/100/25) ramp instruction set. After spinning, the wafer was soft baked at 108° C for 2 minutes to semi-harden the photoresist onto the wafer. Both sides of the wafer were coated with photoresist. Coating both sides ensures that the oxide layer on the bottom side stays intact during top side etching.

*Figure 27: Wafer Spinner*

## Photolithography

The next step was to expose the photoresist. The photoresist was a positive type which means that the area that is exposed to UV radiation will be broken down and removed. The equipment used to expose the photoresist was the Karl Suss MA6/BA6 mask aligner. To select the area that needs to be UV exposed, a photolithography mask was made. What the mask looks like and how it is used can be seen in Figure 29.

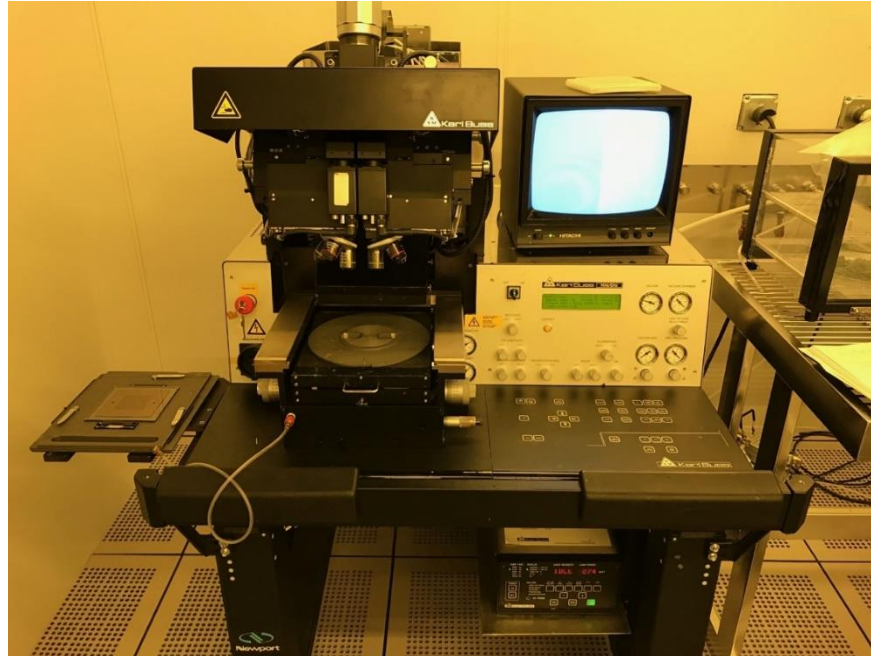

*Figure 28: Mask Aligner*

Because some areas of the wafer are exposed, a mask is needed in order to block the UV radiation. Because the photoresist is a positive resist, the photoresist that the mask does not block will be removed. This mask can be seen in Figure 29

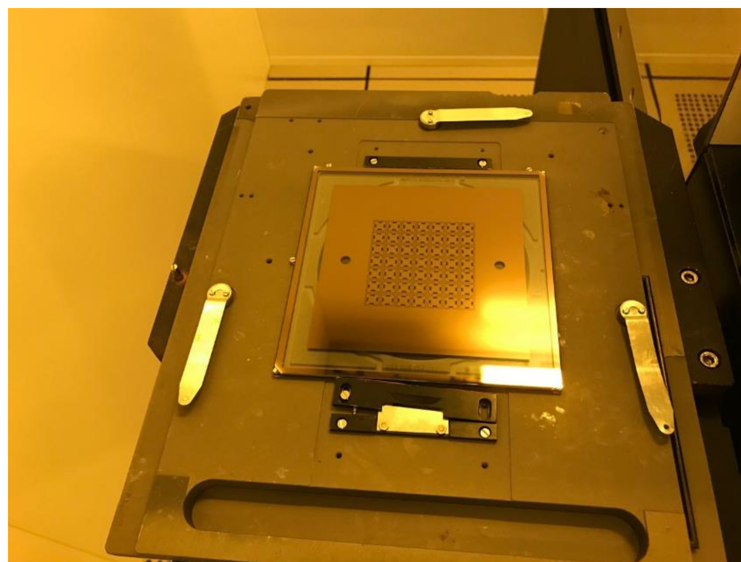

*Figure 29: Wafer Mask*

Instruction set for Photolithography:

1. Warm up lamp
    a. Press “Power”
    b. Press “CP”
    c. Press “Start”
2. Wait until power box reads “IDEA”
    a. Press “Load”
    b. Press “Enter”
    c. Press “Change Mask”
3. Place mask on to mask tray
    a. Press “Enter”
4. Make sure vacuum is holding mask on tray
5. Load tray into tray slot
    a. Press “Change Mask”
6. Turn monitor on and adjust until alignment markers are visible
    a. Press “grab image” the capture overlay image
    b. Press “Load”
7. Open wafer tray and place wafer
    a. Press “Enter”
8. Close wafer tray
    a. Press “Enter”
9. Align markers to wafer markers
10. Adjust exposure time

a. Press “Edit Parameter”

b. Adjust time using directional pad (35 Sec)

c. Pres “edit Parameter”

11. Press “Exposure”

Following these instructions will activate the UV lamp and expose the wafer to the UV radiation. Once exposure is complete, the wafer was extracted from the tray and placed into a development bath of AX400k, 2:1 $H_2O$ for 90 seconds. After development, the wafer was given a Di $H_2O$ rinse and blown dry. The final product can be seen in Figure 30.

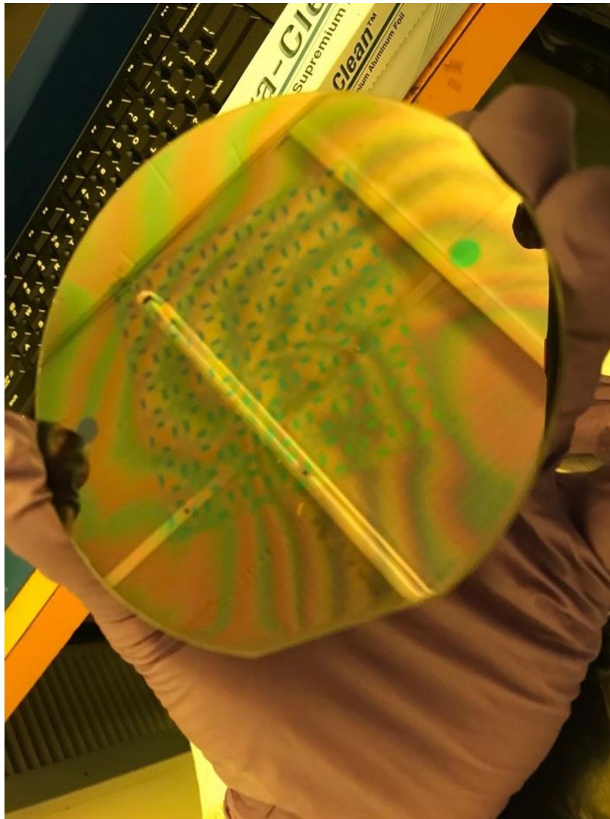


*Figure 30: Wafer w/ Photoresist*

### Oxide Etching

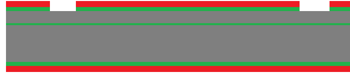

The next step for fabrication was the removal of exposed oxide layer. Under Jeager's silicon wafer cleaning procedure, the removal of hydrous oxide is achieved by submerging the wafer into a Hydrofluoric Acid (HF) deluded bath (BOE). The ideal delusion ratio of HF in the BOE bath is 1:50 [13]. This process is regarded as wet oxide etching.

Determining the quality of the oxide layer is an important aspect; especially when it comes to oxide etching. Any residual oxide on the wafer surface will produce quality issues farther down the process. Characterization of oxide thickness or lack of thereof was preformed through optical inspection. The measurand is the visible wavelength that the wafer emits. Silicon dioxide is mostly a transparent material of which visible wavelengths can pass through. The silicon underneath the silicon dioxide is not transparent and will reflect remaining light rays. The constructive interference between the wavelength reflected from the silicon dioxide and silicon layer produces a visible wavelength unique to the thickness of the silicon dioxide layer [24]. The relation between the thickness of the oxide layer and the resulting wavelength can be determined with

$$2X_o = k\lambda/n, \qquad \text{Eq 34}$$

Where $X_o$ is the oxide layer thickness, k any integer greater than 0, n is the refractive index of silicon dioxide which is equal to 1.46, and $\lambda$ is the wavelength [13]. If no silicon dioxide is present on the wafer, the emitting color of the wafer will be grey with not secondary hue. The following instruction set was taken until not secondary colors were visible in the target areas. The final product can be observed in Figure 31.

Oxide Etch Instructions:

1. Dip wafer into DI $H_2O$
2. Dip wafer into BOE for 2 minutes and agitate bath by tapping lightly on container
3. Remove wafer form BOE bath and dip in DI $H_2O$
4. Rinse wafer in sink
5. Air dry wafer
6. Repeat until grey silicon is fully exposed

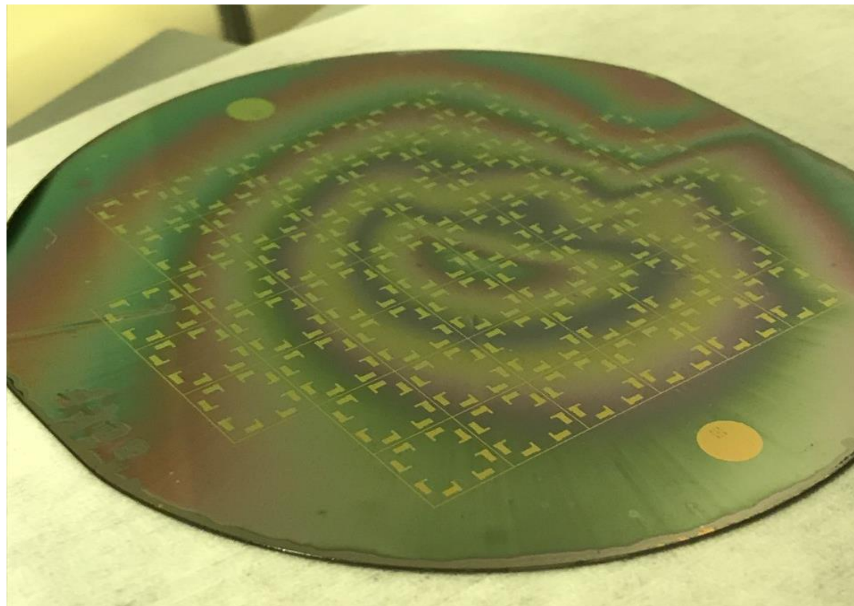

*Figure 31: Wafer w/ Exposed Silicon*

Under a microscope, enhances inspection was taken place. Under a microscope, the grey surface will reflect the light from the instruments lamp. A control wafer should be used to gauge the color of bear silicon. For this study, the silicon surface emitted a baby blue hue while the photoresist and silicon dioxide emitted a red violet. The microscope image can be seen in Figure 32.

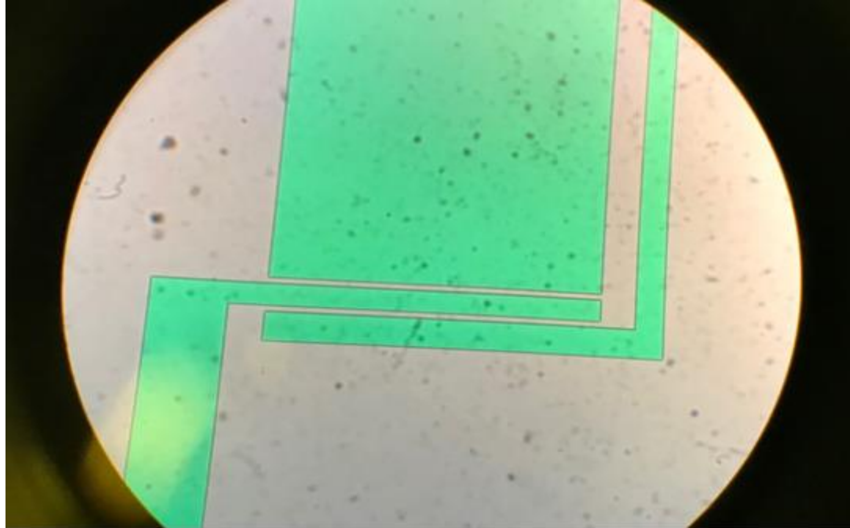

*Figure 32: Exposed Silicon under Microscope*

## Silicon Etching

With the oxide layer stripped in the target regions, the next step was to etch the silicon. Etching was done using a Deep Reactive Ion Etching (DRIE) STS etcher. STS etcher removes silicon with high depth to length ratio (aspect ratio) through a two-stage cycle process inside a vacuum chamber. General setup of the chamber can be seen Figure 33. First stage pumps SF8 plasma into the chamber. The plasma immediately removes the exposed silicon from the wafer. Etching happens in both vertical and horizontal direction. Before undercutting occurs, the etcher stops the etching stage and transitions to the second stage, passivation. This stage pumps a gas comprising of C4F4 into the chamber and creates a polymer layer of the exposed silicon. When the etching stage starts again, the horizontal layer is removed and the silicon underneath is etched. The vertical polymer layer is not removed and protects the silicon from farther etching.

This cycle repeats until a desire depth into the silicon wafer is meet [25]. The process of etching and removing can be seen in Figure 34.

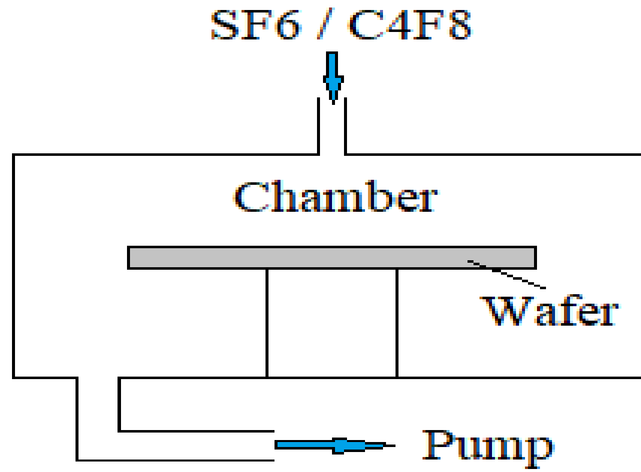


*Figure 33: DRIE Chamber*

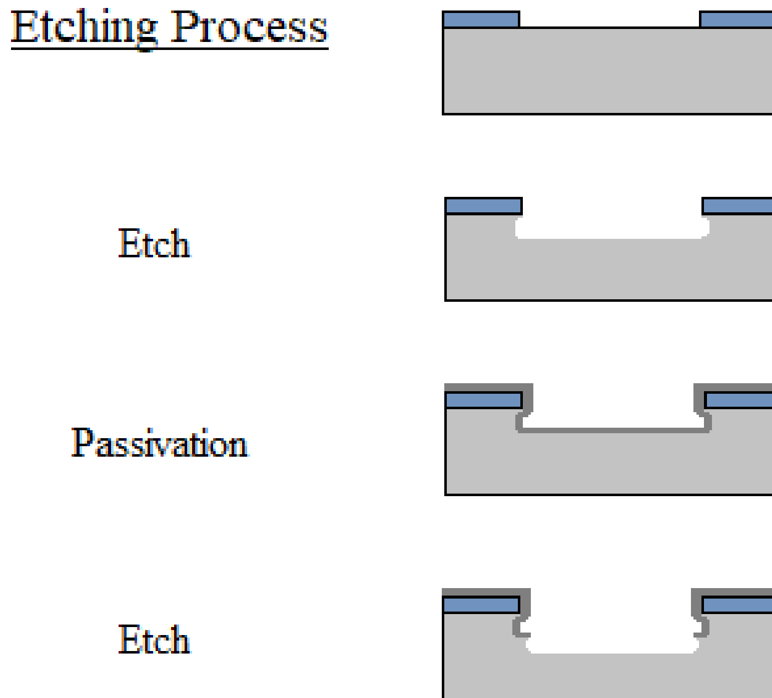


*Figure 34: Etching Process*

STS etching instructions:

1. Select Passivation/etch Profile (MoranSOI)
2. Select “Recipe” to edit
    a. Set number of cycles to 100, check max flow is set to 40, min flow to 10.
3. “vent” chamber
4. Wait for pressure to reach 700 Tor
5. Load wafer in far tray
6. “pump and map”
7. Wait for load button to be ready
8. “load”
9. Wait until wafer is loaded
10. “process”

Etching Process begins

11. After etching press “unload”
12. “Vent” after wafer is back on far tray
13. Rotate wafer 180°
14. Start step 6 and repeat until desired depth is reached

If instructions are followed correctly, the STS etcher will remove the silicon from the wafer. This process was executed until reaching the box layer. The final product can be seen in Figure 35.

*Figure 35: Top Side Etched Wafer*

PR Stripping

Once the desired amount of silicon was etched, the next step was to remove the photoresist that was used to protect the oxide layer and silicon underneath. This process is similar to cleaning the wafer. The wafer was given an acetone, methanol, and isopropanol rinse. A deionized water rinse and $N_2$ blow dry followed. The wafer was then placed in an oven for 15 minutes at 100° C to remove moisture.

Bottom side Processing

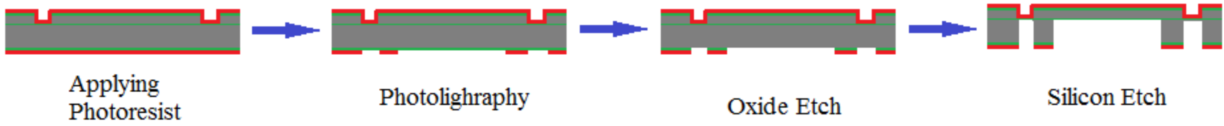


The latter half of the fabrication process focuses on etching the handle layer of the wafer. This process is the same as the device layer starting at the “Applying Photoresist” step. The only difference between the device side processing and the handle layer is the addition of a second wafer that is attached to the device side of the wafer via photoresist. This second wafer is attached during the "Applying Photoresist” step and serves to hold the isolator when they release on the “Silicon Etch” step. The final back side etch can be seen in Figure 36.

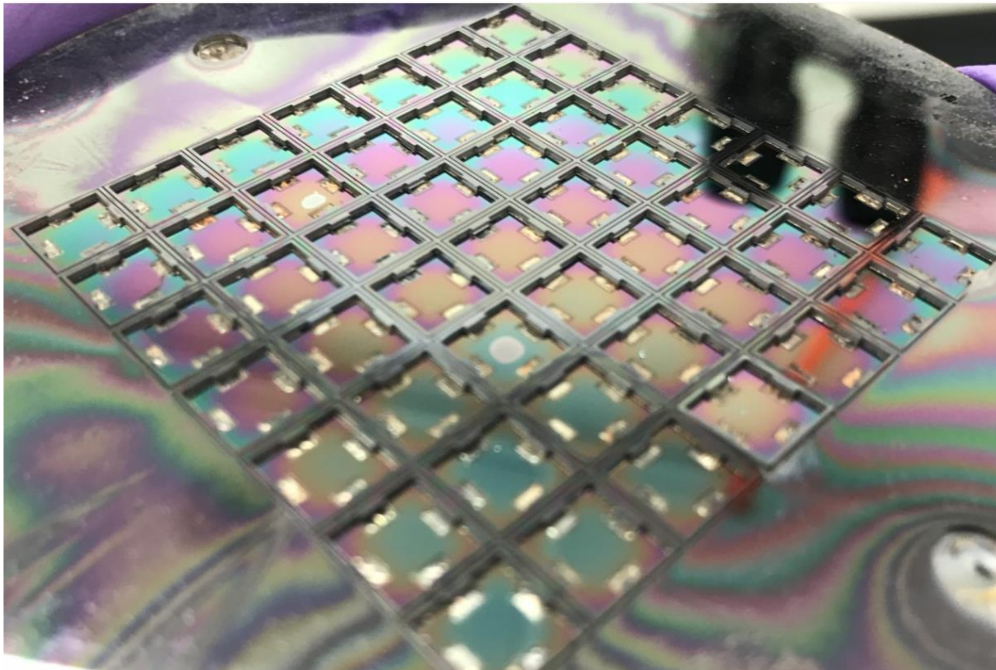

*Figure 36: Bottom Side Etched Wafer*

Photoresist Strip and Release

The final step in manufacturing the isolators is stripping the photoresist. This strip will release the isolators from the wafer. This process is done by submerging the wafer into an acetone bath for several hours or when all of the isolators detach from the wafer. Once the isolators are fully detached, they were given an acetone, methanol, and isopropanol rinse, followed by a deionized water rinse and $N_2$ blow dry.

Post-Manufacturing Quality Control

After fabrication, the etch isolator was inspected. The final I3 and I9 isolators can be seen in Figures 37 and 38.

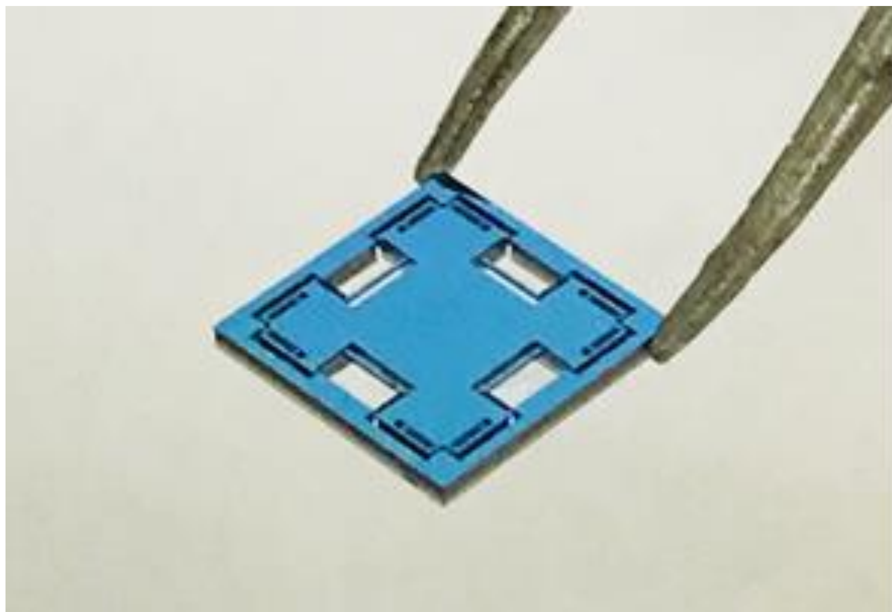

*Figure 37: I3 Isolator Complete*

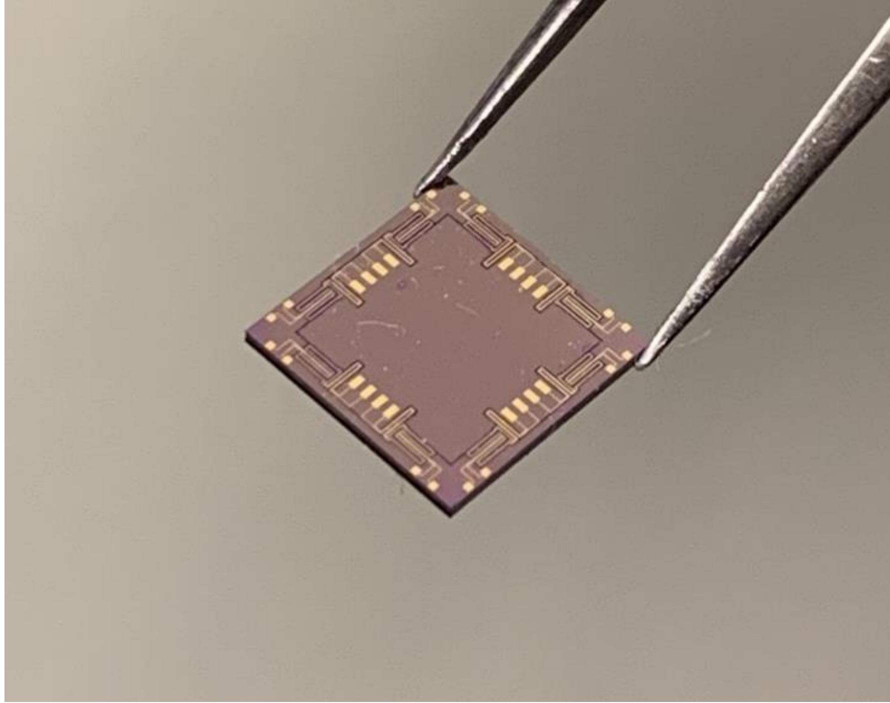

*Figure 38: I9 Isolator Complete*

## Additive Manufacturing

The 3D printing process takes a unique approach to the fabrication when compared to traditional fabrication. Instead of subtracting material, printing fabricates objects through additive manufacturing. The process begins with designing a digital model. This is done using SolidWorks. The design can be seen in Figure 39. The concept of this design is to suspend a platform in the middle of a frame with eight leaf springs. The platform is in the area that holds the sensor and the frame attaches to the larger body. The leaf springs will be made of a photo-polymer material that will have spring and dampening properties.

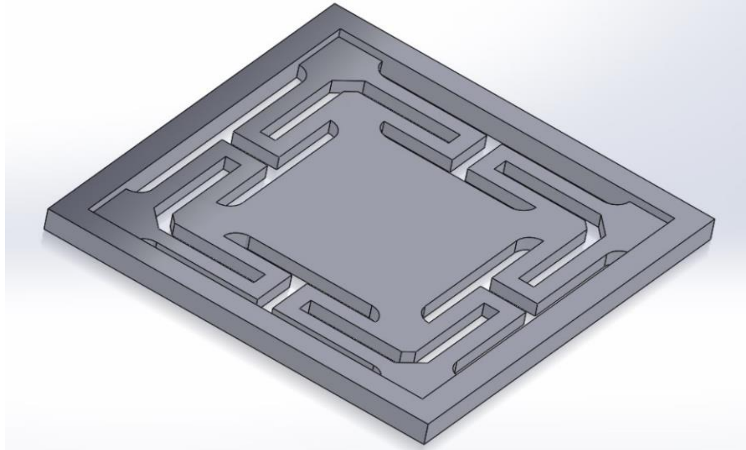

*Figure 39: Printed Isolator*

After confirming that the design had the desired damped natural frequency, the 3D model was rendered into a .STL print file. The .STL file is the file that was loaded into the 3D printer. The printer used in this study is the Formlabs' Form 2. The Form 2 is a part of the latest generation of 3D printers. It operates on stereolithography technology. Stereolithography or SLA 3D printing uses a UV laser to cure a liquid photopolymer resin into solid material [26]. The Form 2 printer can be seen in Figure 40.

*Figure 40: FormLab's Form 2 Printer*

The process of printing the fixture took approximately 4 hours to complete. After printing, the isolators were dipped into a rubbing alcohol bath and further exposed to UV radiation. The additional exposure hardened the isolators. Light sanding was applied to each of the isolators in order to remove excess buildup from the print supports. The 3D printed isolator can be seen in Figure 41.

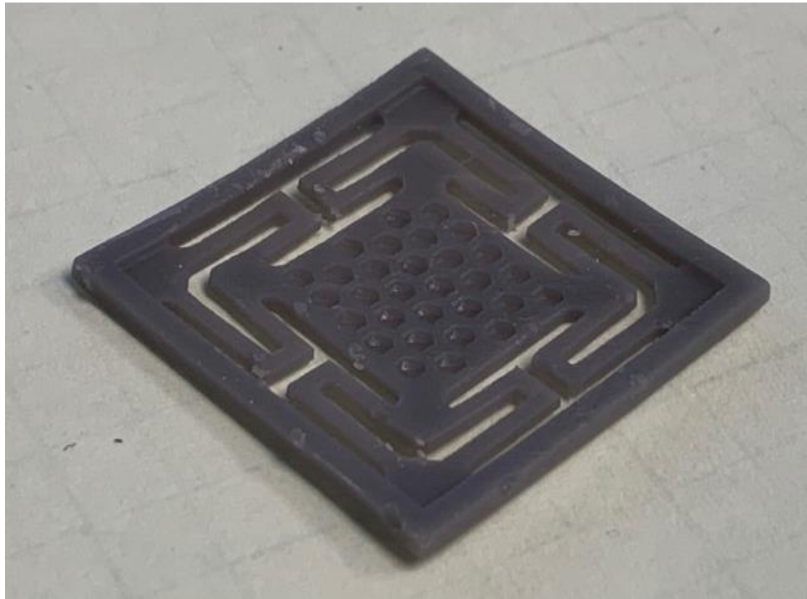

*Figure 41: Printed Isolator Complete*

## Testing

The isolators have been fabricated. The next step was to evaluate their responses through testing. Testing determined if theoretical behavior of the isolator compares to its actual behavior. The first step in testing is to identify the goal. The purpose of the test is to find the natural frequency of a mechanical isolator with a simulated mass attached to it. To acquire the natural frequency, a characteristic of it must be traceable. Looking back at the transmissibility chart, one can see that resonant frequency is reached when the displacement ratio (q/u) is at its maximum. If the distance

between the components were measured, the natural frequency could be found. Since the system is based on a base excitation model, the best locations to trace would be the frame of the isolator and the attached mass.

Now that the goal has be identified, the next step is to develop a way to acquire it. This can be done with a device known as a laser vibrometer. A laser vibrometer system works by emitting two parallel laser beams onto a mechanical system. The lasers will make contact with two different components. The laser beams will reflect off the surfaces of the components and return to the emitters. The emitters will then output signals to an analyzer. The output signals are the instantaneous measurements between the emitters and the surfaces of the target components. The analyzer will take the two signals from the emitters and generate the instantaneous distance between the components with respect to a single axis. It will store this measurement and assign it to the frequency that is being applied to the mechanical system. This setup is shown in Figure 42.

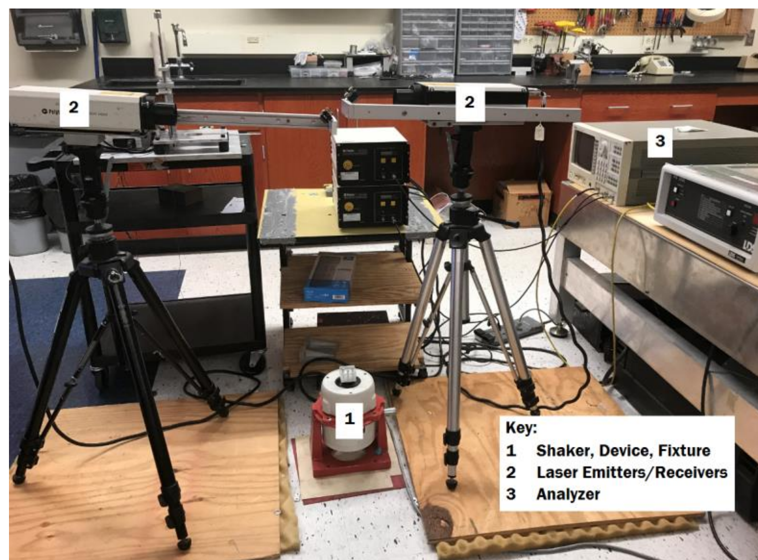


*Figure 42: Laser Vibrometer Setup*

Because the goal is to find the maximum distance between oscillating components, a range of frequencies was needed to be tested. To set the frequency range and apply it to the isolator, the analyzer has control of a mechanical shaker, which is a device that vibrates the test assembly. Because the isolators are so small, there was a need for adaptors between the isolators and the shaker. This adaptor is known as the fixture and is a component that will fix the isolator's frame and act as a continuation of the base excitation. The fixture's motion will be measured by the laser vibrometer. The fixtures for the printed isolators can be seen in Figures 45 and 46.

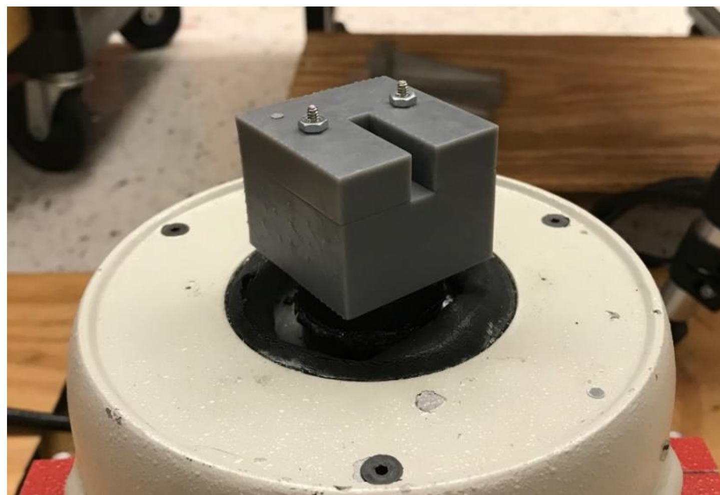

*Figure 43: Fixture on Shaker (Silicon Isolator)*

To lock the isolator to the fixture, the fixture will follow a clamshell design where two pieces of material will be bolted together with the isolator sandwich between them. The isolator will be locked into a recess cut into one of the two pieces. The recess will also have a cavity at its center to allow the isolator to oscillate along its intended axis. The other piece will also have an open cavity which allows direct line of sight between the proof mass on top of the isolator and one of the laser emitters. Cylindrical studs and recesses will be included in the top and bottom half of the fixture. These studs and recesses will be used to align the two halves precisely together. A design for the fixture is shown Figure 44.

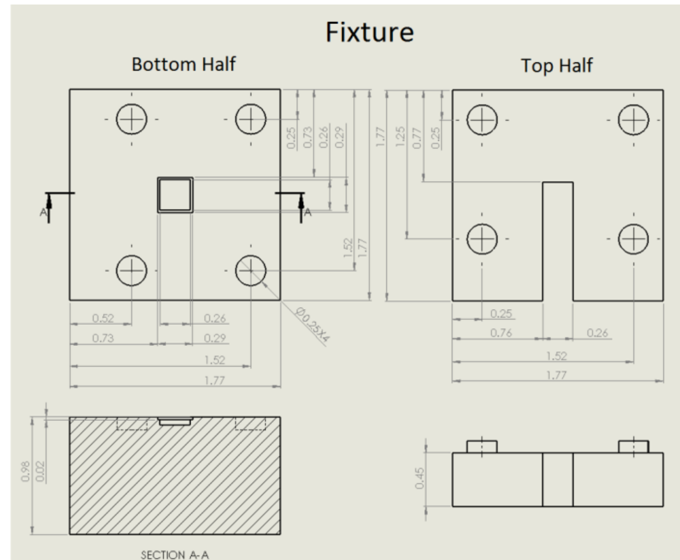


*Figure 44: Fixture Design*

The fabrication process began with a developing a digital model. This was done in Solidworks. The 3D model was then rendered into a .STL print file and loaded into the Formlabs' Form 2 printer. The printing process took approximately 14 hour to complete. After printing, the components were lightly sanded to remove excess buildup from the print supports. The final step was to drill a hole and insert the threaded bolt into the bottom piece. The 3D printed fixture is shown in Figure 45.

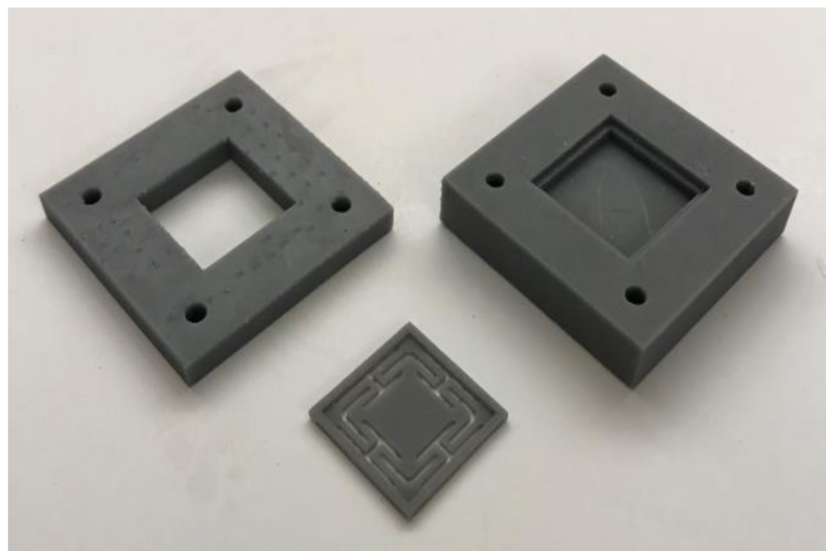

*Figure 45: Isolator Fixture (Printed Isolator)*

The other component that was measured was the proof mass that set on the isolator. As mention earlier, the proof mass was a small block of aluminum that simulates the mass of the sensor. The isolator inside the fixture and holding the proof mass can be seen in Figure 46. When conducting a test, the analyzer will sweep across a large range of frequencies and takes a measurement for each frequency divisible by 8. This division is based on the smallest resolution that the analyzer can achieve. After the sweep, the analyzer will store all the information collected from that sweep into a single sample. This process will repeat until 250 samples have been collected. The analyzer will average the 250 samples into a single set.

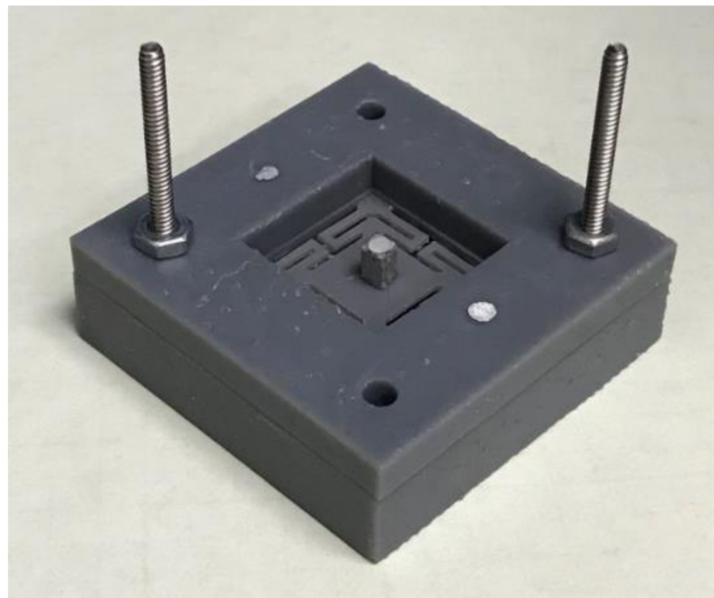

*Figure 46: Fixture Assembled*

## Results

Several isolator configurations were analyzed with the above mentioned test setup. Configurations include I3 with no damping component, I9 with no damping component, printed isolator with varying material and no damper, I9 with PDMS damper, and I9 with Sorbothane damper. Attempts to test I3 with dampers were unsuccessful due to the extreme fragile nature of the isolator and the consistent tendency to fracture when damper components were attached. Any moderate compressive force that the damping component administered to the I3 surpassed the fracture point of the I3 springs. The following results are the raw responses for each configuration. The responses are captured from 200 to 6600 Hz. The high frequency testing was to ensure that no additional resonant frequencies excite in the system. Addition resonant frequencies would indicate that off axis excitation was occurring in the system. Off axis modes are generally undesirable. These responses for the silicon-based isolators can be seen in the following Figures:

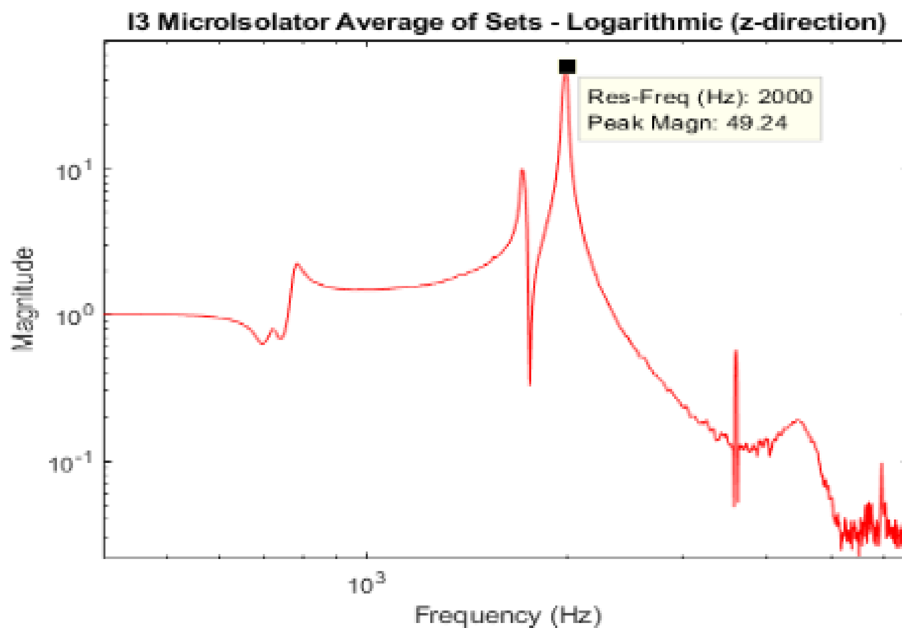


*Figure 47: I3 Undamped Results*

The I3 isolator showed a response analogous to the transmissibility plot from the simulated model. Unfortunately, the response was well outside that target goals. The resonant frequency was 2.0 kHz with a peak magnitude of 49.2. Another issue was the isolator was found to be highly delicate, even without an attached damping component. Multiple isolators were destroyed in the attempt to evaluate them. Another difficultly factor was the limited real estate of the platform. This made it difficult to mount the proof mass. Difficultly in mounting the proof mass is a clear indication that mounting accelerometers would be a challenging obstacle. Because of the limitations of the I3, the I9 was developed. The I9 offered a larger platform for the accelerometer and is structurally more robust.

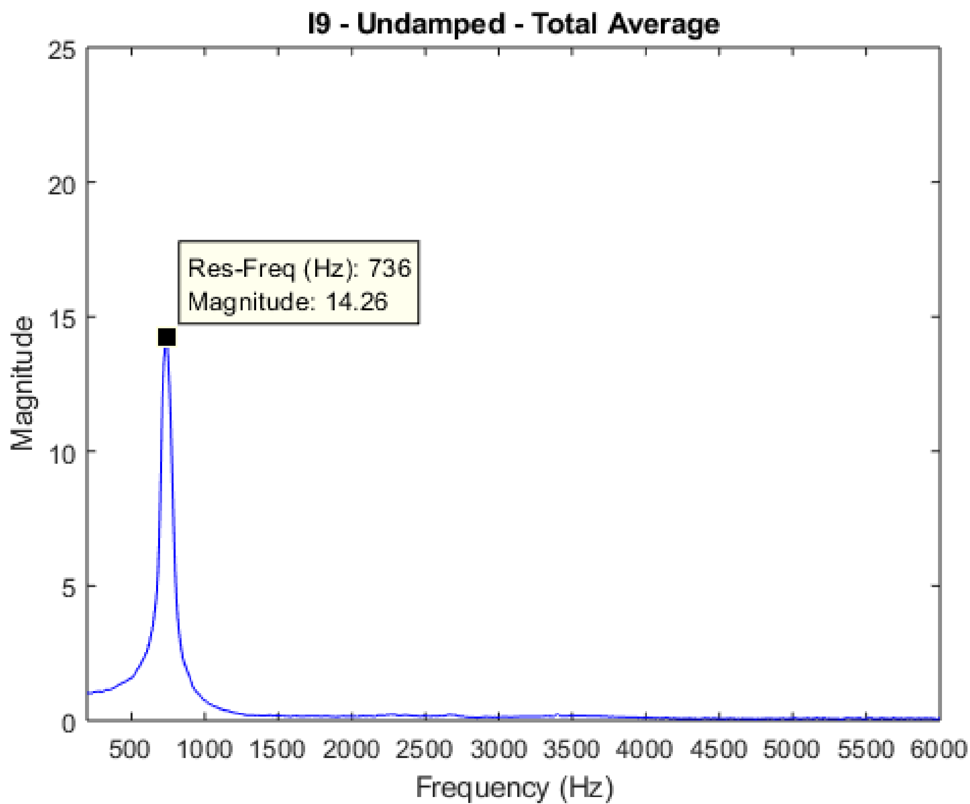


*Figure 48: I9 Undamped Results*

The undamped I9 configuration showed a promising transmissibility response during shaker excitation. The resonant frequency was found to be 0.736 Hz. This response was in line with the simulated model; having a deviation error of only 1.98%. As mentioned in the damping section of this study, exhibiting a sub target value for I9's resonant frequency was an intentional effort. Native sub 1.0 kHz response allows offset of damping components that would increase the resonant frequency with the inclusion of their stiffness. The high native transmissibility peak of 14.26 indicated that a damping component was necessary for the I9. The following result are the responses of I9 with varying types of damper components.

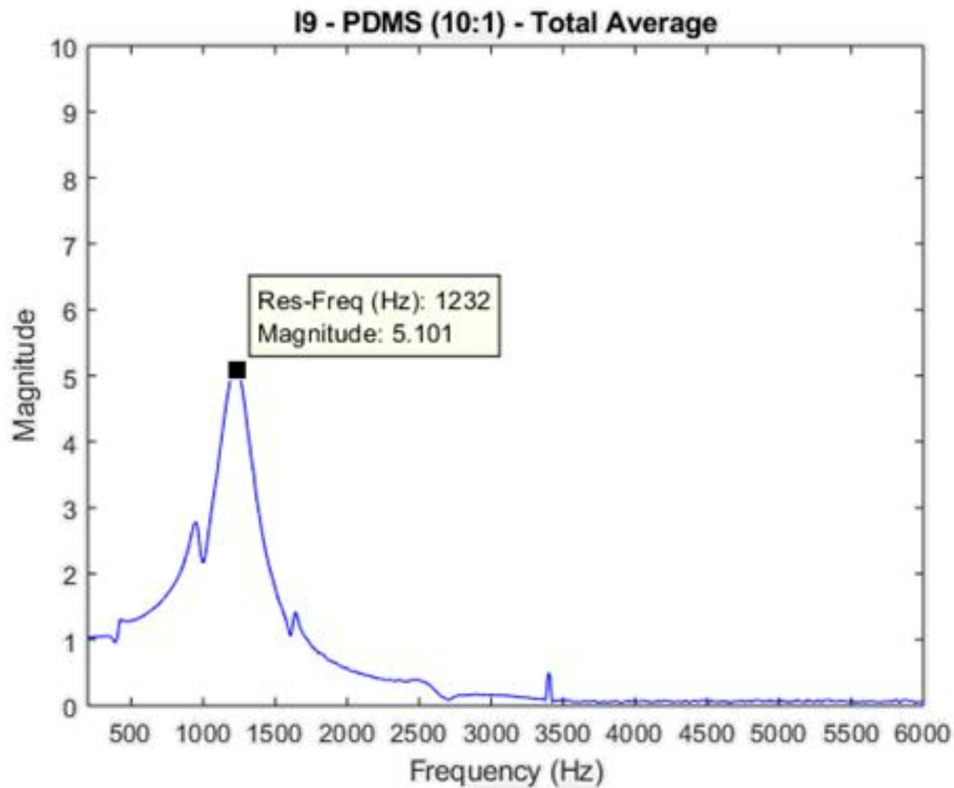


*Figure 49: I9 PDMS Results*

The addition of a 2.54 mm cubic PDMS (10:1) had a substantial improvement in the I9 transmissibility response. The transmissibility peak dropped to 5.101 while the resonant frequency rose to 1.232 kHz. As mentioned in the last section, the rise in resonant frequency was due to the stiffness of damping material. This response was almost within the mission parameters. The only visible issue is the additional peaks that are found before and after the transmissibility peak. These additional peaks indicate additional modes being excited. This problem was believed to have been caused by improper alignment of the damping component.

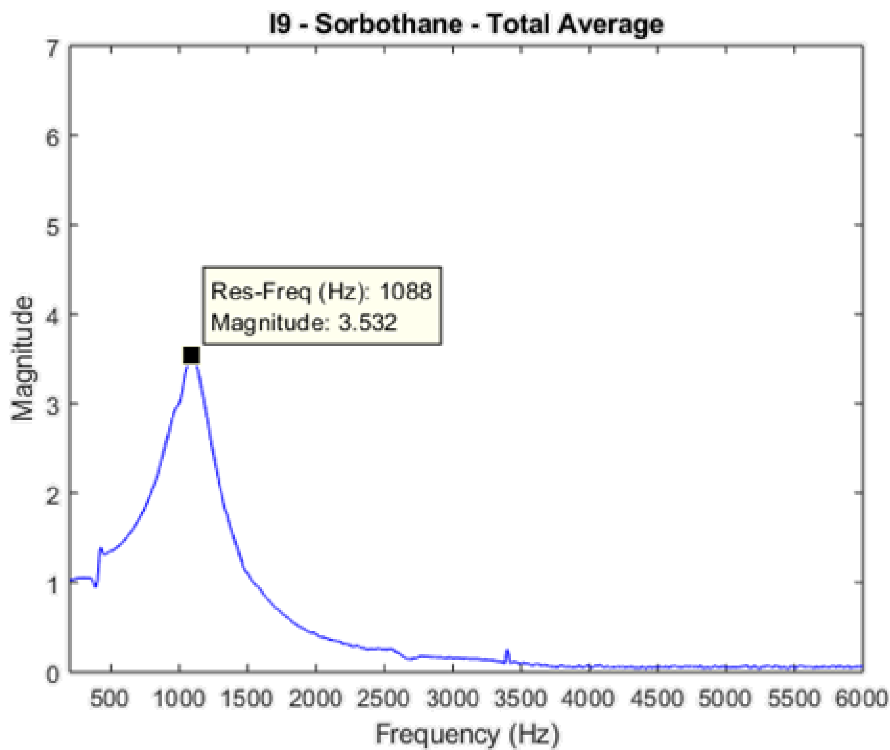


*Figure 50: I9 Sorbothane Results*

The next damping component that was attached to the I9 isolator was the Sorbothane (Duro 70). The component was packaged in a 2.54mmx2.54mmx2.54mm cube. Just like the PDMS, the sorbothane showed a positive effect in the I9's transmissibility response. The resonant frequency

was 1.088 kHz with a peak magnitude of 3.535. This response is well within the objective parameters. Another positive quality of the response profile is the lack of additional peaks. A single peak in the transmissivity profile indicates that only one mode is being excited.

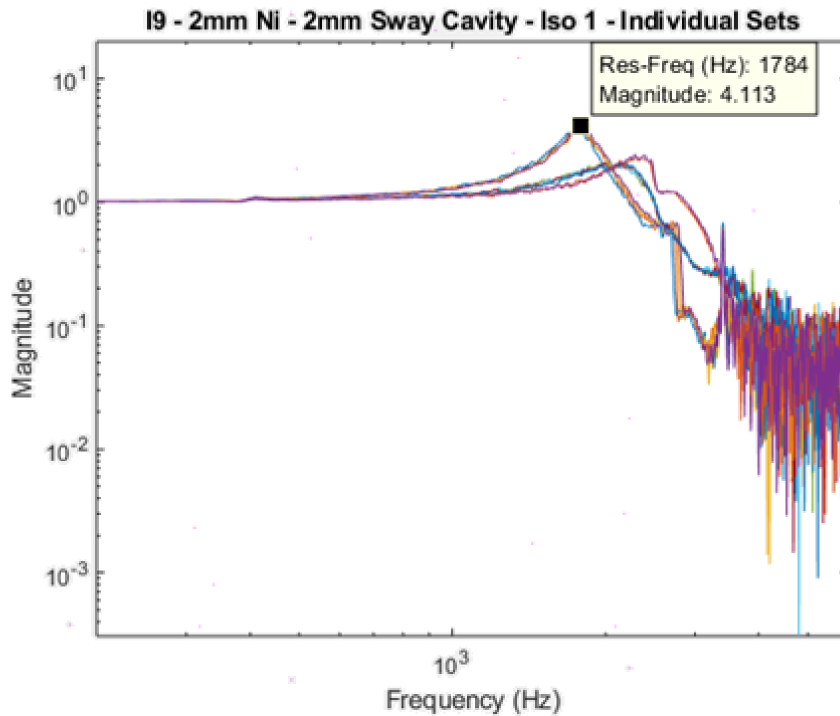


*Figure 51: I9 w/ Ni Mesh*

The I9 isolator suffered consistency issues when equipped with the nickel mesh damper. Resonant frequencies spanned from 0.968 kHz to 1.784 kHz. Transmissibility peaks, with and span from 1.051 to 4.113, also suffered in the area of consistency. Additional modes of excitement were also observed. The lack of consistency is believed to be from the lack of uniformity within the material. Nickel mesh has been observed to not retain its original properties when compressed or folded. This constant change in geometry may induce inconsistent damping and create varying mechanical properties within the system. The next set of test result were from the printed isolator.

*Figure 52: Grey Printed Isolator Results*

The first test results were the printed isolator made of the grey resin. Due to a wide variation in responses across several isolators, the data for the 3D printed isolators were split into averages for each of the isolators, rather than a single average. Five isolators were tested and the transmissibility response for each is seen in Figure 52. All isolators exhibited a resonant frequency near 1.0 kHz with a Transmissibility peak ranging from 12.2 to 19.1. Although the resonant frequency is in line with the target frequency, the peak magnitude is well above the target value. Due to the interest of packaging 3D printed isolators as a homogenous unit, other printable materials were explored.

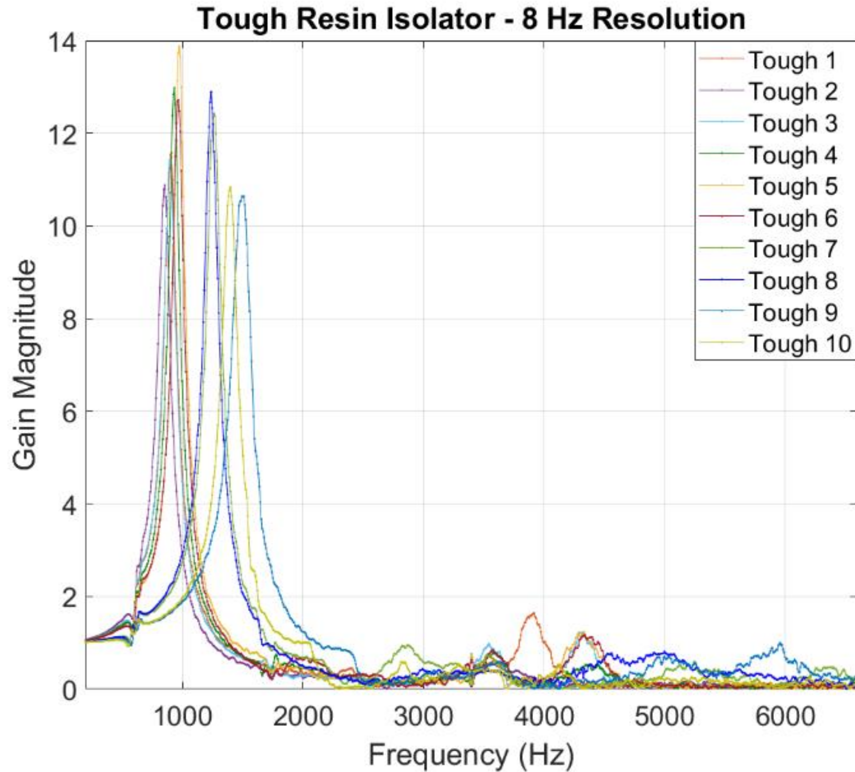


*Figure 53: Tough Printed Isolator Result*

The first alternative material explored was FormLab's tough resin. The isolators were manufactured using the same method as with the grey resin. The material properties can be found in [21]. The resonant frequency responses were found to be between 0.970 to 1.450 kHz with peak magnitude from 10.5 to 13.9. Although the transmissibility peak was lowered, the large range in resonant frequencies is not ideal for a final product. Additional modes were also observed post transmissibility peak. This indicated that rotational modes may have been present during excitation. Other printable materials from FormLabs are available and may be considered in future efforts.

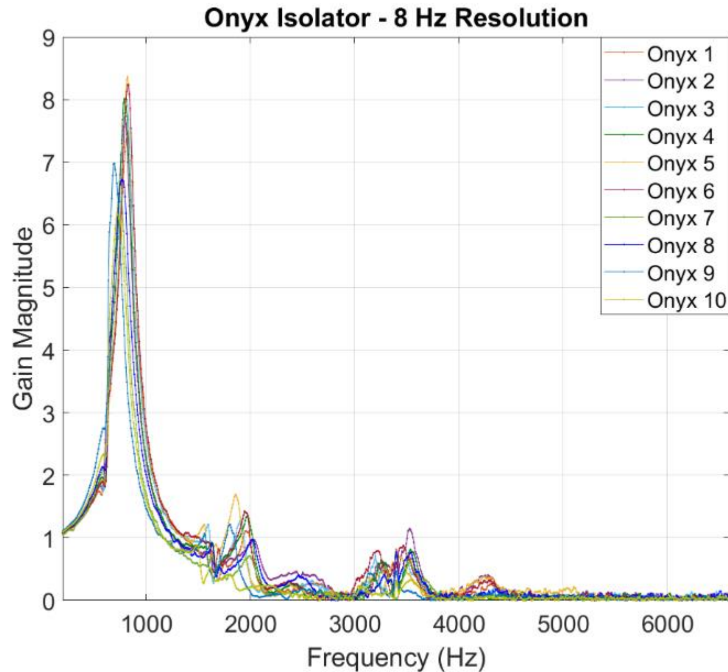


*Figure 54: Onyx Printed Isolator Result*

The last alternative material explored was Onyx filament. This isolator was fabricated via filament deposition manufacturing (FDM). FDM works by heating and stacking thermal plastic filament to form an object. The material strength of the filament is not as strong as the photopolymer, but it is still strong enough to serve as an isolator. The responses across the tested isolators were consist. The resonant frequency was found to be 0.824 kHz with a peak transmissibility around 8.1. Based on the responses, the I9 with PDMS and sorbothane damping element performed as desired with resonant frequencies around the 1.0 kHz mark and peak transmissivities near of below 5.0. The undamped I9 preformed as expected with a sub 1.0 kHz response and magnitude above 5. The general response of the Onyx printed isolator was the best out of the 3D printed isolators; however, it still did not meet the transmissibility peak requirement. Due to the failure of all 3D printed isolators, the inclusion of a damping element may be required just as it is for the silicon based isolators.

# Conclusion

MEMS devices, such as accelerometers and gyroscopes, have been observed to have vulnerabilities to high frequency mechanical vibrations. These vulnerabilities are problematic as many of these devices are deployed in harsh environments that can spawn such frequencies. This effort studied and explained the nature of the problem and generated a theoretical solution. The solution took the form of mechanical isolators. Passive isolators provide protection to the MEMS devices by acting as a low pass filter and attenuating the felt response of disruptive high frequencies. Two approaches of the solution were introduced. One approach was silicon-based isolators with secondary damping elements equipped. The other approach was a polymer-based 3D printed isolator with integrated damping elements.

Isolators were designed around both approaches. Computer aided finite element analysis software was used to adjust and verify the expected response for each isolator. Silicon based isolators were fabricated with the method known as microfabrication and polymer isolators were fabricated through additive manufacturing. Two designs of silicon-based isolators were developed, I3 and I9. The printed isolator was made with various materials.

The isolators were evaluated via subjecting each to a simulated harsh environment. The environment consisted of a mechanical shaker that induced a wide frequency range into fixtures that housed the isolators. The transmissibility response for each isolator and its configuration was captured via laser vibrometer. Based on the test results, I9 equipped with 2.54 mm cubic damping component made of PDMS (10:1) and Sorbothane exhibited adequate or nor adequate isolation performance. Printed isolators were found to struggle in isolation performance with high transmissibility peak and inconsistent resonant frequencies. Refining the print process and the inclusion of secondary damping elements in the system may improve isolation performance.

## Future Work

The next stage for this effort is to continue investigating the printed isolators and integrating an additional damping element. When using the undamped I9 response as a point of comparison, the addition of a damping material should lower the transmissibility peak of the printed isolators. If the printed isolator is feasible with secondary damping elements, the next stage should be to integrate electrical traces on top of the isolator for accelerometers or other sensitive MEMS devices. The silicon-based isolators have shown compete capability to attenuate high frequencies. Testing I9 with additional damping component should also be considered. The additional damping components include new geometries and compositions of PDMS and Sorbothane. Nickel and copper mesh may still prove to be useful for the I9 isolator and should be further explored. The next stage for the silicon isolators will be to utilizes the electrical traces that are on the current I9's. Testing live devices on both isolators will require new test fixtures to be developed. This new fixture should accommodate an interface between the active components and the system outside of the fixture. This capability will allow for devices to function and provide data output during testing. The last stage will be to evaluate the isolator with various MEMS devices in both simulated and real world environments.

References


[1] Legaza, V., “Dynamics of Vibration Isolation System with a Ball Vibration Absorber.” *International Applied Mechanics*, Vol. 54, No. 5, September, 2018. Springer, https://link.springer.com/content/pdf/10.1007/s10778-018-0912-0.pdf

[2] Půst, L. “Determining the resonance frequencies of forced vibrations of turbogenerators with foundations.” *Experimental Mechanics* **7,** 265–271 (1967). https://doi.org/10.1007/BF02326998

[3] Beer, Ferdinand. Jhnston Jr, R. Dewolf, John. Maqurek, David. *“Mehcanics of Materials.”* Ed. 6, McGraw hill, New York, NY, 2012

[4] Stephen. Ensell,Graham. Kraft, Michael. White, Neil. *“MEMS Mechanical Sensors.”* Boston. Artech House, Inc. 2004

[5] Yang, et al. “A Resonant Z-Axis Aluminum Nitride Thin-Film Piezoelectric MEMS Accelerometer.” *Multidisciplinary Digital Publishing Institute*, 6 Sept. 2019, *MDPI*, www.mdpi.com/2072-666X/10/9/589/htm.

[6] Fraden, Jacob. *“Handbook of Modern Sensors.”* New York, *Springer,* 2010

[7] Palm III, William. “System Dynamics, Third Edition.” New York NY, McGrawHill, 2014.

[8] Kim, Jin. Dean, Robert. Flowers, George. Chen, Chen. “Active Vibration Control and isolation of Micromachined Devices.” *Journal of Mechanical Design,* Vol. 131, ASME, Sept. 2009.

[9] Shi, Xiang. Zhu, Songye. “A Comparative Study of Vibration Isolation Performance using Negative Stiffness and Inerter Dampers.” *Franklin Institute*. July 2019. pp.7923. *ScienceDirect*.

[10] Wang. Bochao, Kari, L. “Modeling and vibration control of a smart vibration isolation system based on magneto-sensitive rubber.” *Smart Materials and Structures.* Vol. 28, 2019. *IOPScience.* https://iopscience.iop.org/article/10.1088/1361-665X/ab1ab4/pdf

[11] Voldman, Joel. “Microfabrication in Biology and Medicine.” *MIT*, 1999, www.rle.mit.edu/biomicro/reprints/jvoldman_annrev.pdf.

[12] Jones E.D., Miller L.S., Mullin J.B. “Control of Semiconductor Conductivity by Doping”. *Electronic Materials*. Springer, Boston, MA, 1991.

[13] Jaeger, Richard. “Introduction to Microelectronic Fabrication.” Vol. 5 Ed. 2, Saddle River, New Jersey, Prentice Hall, 2002

[14] Enstrom, R. and Doane, D., “A finite Element Solution for Stress and Deflection in a Centrally Laded Silicon Wafer,” *Semiconductor Characterization Techniques*, 1978. [online] Google

[15] Shahrubudin, N., et al. “An Overview on 3D Printing Technology: Technological, Materials, and Applications.” *Procedia Manufacturing*, vol. 35, 2019, pp. 1286–1296, 10.1016/j.promfg.2019.06.089.

[16] Wohlers, Terry. “Early Research & Development.” *Wohlers Associates*. 2005. www.wohlersassociates.com/history.pdf. Access July 14 2019.

[17] Sawant, Rogit. Kakade Prasad. "3D Printing Market Outlook – 2025. " *SE: Electronic Systems and Devices.* Vol. A00145. pp. 163, Oct 2018, *Allied Market Research,* https://www.alliedmarketresearch.com/3d-printing-market

[18] Pereira, Tanisha, et al. "A Comparison of Traditional Manufacturing vs Additive Manufacturing, the Best Method for the Job." *Procedia Manufacturing*, Apr. 2019, *Elsevier,* www.sciencedirect.com/science/article/pii/S2351978919300332

[19] Chen, Zhangwei, et al. "3D Printing of Ceramics: A Review." *Journal of the European Ceramic Society,* Nov. 2018, *Elsevier,* https://www.sciencedirect.com/science/article/pii/S0955221918306782

[20] Baskaran, Vivek, et al. "Current Applications and Future Perspectives of the Use of 3D Printing in Anatomical Training and Neurosurgery." *Frontiers in Neuroanatomy*, vol. 10, 24 June 2016

[21] "Materials for High-Resolution Rapid Prototyping." *FormLabs*, 2019 https://archive-media.formlabs.com/upload/XL-DataSheet.pdf

[22] Yao, S. K., et al. "The Plastic and Creep Behavior of Silicon Microstructure at High Temperature." *The Plastic and Creep Behavior of Silicon Microstructure at High Temperature - IEEE Conference Publication*, IEEE, 10 Oct. 2013, ieeexplore.ieee.org/document/6626726.

[23] Liu, Haiyun. Wang, Lei, "Measurements of thermal conductivity and the coefficient of thermal expansion for polysilicon thin films by using double-clamped beams," *Journal of Micromechanics and Microengineering*, Vol. 28, No. 1, Dec 2017, https://iopscience.iop.org/article/10.1088/1361-6439/aa9d29/meta#references

[24] Huen, Tony. "Reflectance of Thinly Oxidized Silicon at Normal Incidence." *Applied Optics*, June 1979, *Optical Society of America,* www.osapublishing.org/ao/abstract.cfm?uri=ao-18-12-1927.

[25] Spearing, Mark. "Key Processes for Fabrication of the MIT Microengine ." *Research Gate*, R&T Organization, 28 Aug. 2014.

[26] Liska, R., Schuster, M., Inführ, R., Turecek, C., Fritscher, C., Seidl, B., Schmidt, V., Kuna, L., Haase, A., Varga, F., Lichtenegger, H. and Stampfl, J., "Photopolymers For Rapid Prototyping." *Journal of Coatings Technology and Research,* January 2007, pp. 505-510, *ResearchGate,* https://www.researchgate.net/publication/227256261_Photopolymers_for_rapid_prototyping

[27] Bottenfield B., Bond, A., Kranz, M., Dean, R., and Adams, M. "Variations in Micromachined Isolator Geometries for Sensor Performance in Harsh Environments". *IEEE Transactions on Components, Packaging and Manufacturing Technology*. 2020; Vol. 10, No. 4